Active Site Models for the Cu$_A$ Site of Peptidylglycine α-Hydroxylating Monooxygenase and Dopamine β-Monooxygenase

Atsushi Kunishita,[†] Mehmed Z. Ertem,[‡] Yuri Okubo,[†] Tetsuro Tano,[†] Hideki Sugimoto,[†] Kei Ohkubo,[†] Nobutaka Fujieda,[†] Shunichi Fukuzumi,[†,§] Christopher J. Cramer,*[,‡] and Shinobu Itoh*[,†]

[†]Department of Material and Life Science, Division of Advanced Science and Biotechnology, Graduate School of Engineering, Osaka University, 2-1 Yamada-oka, Suita, Osaka 565-0871, Japan

[‡]Department of Chemistry, Supercomputing Institute, and Chemical Theory Center, University of Minnesota, 207 Pleasant Street SE, Minneapolis, Minnesota 55455, United States

[§]Department of Bioinspired Science, Ewha Womans University, Seoul 120-750, Korea

S Supporting Information

ABSTRACT: A mononuclear copper(II) superoxo species has been invoked as the key reactive intermediate in aliphatic substrate hydroxylation by copper monooxygenases such as peptidylglycine α-hydroxylating monooxygenase (PHM), dopamine β-monooxygenase (DβM), and tyramine β-monooxygenase (TβM). We have recently developed a mononuclear copper(II) end-on superoxo complex using a N-[2-(2-pyridyl)ethyl]-1,5-diazacyclooctane tridentate ligand, the structure of which is similar to the four-coordinate distorted *tetrahedral* geometry of the copper-dioxygen adduct found in the oxy-form of PHM (Prigge, S. T.; Eipper, B. A.; Mains, R. E.; Amzel, L. M. *Science* 2004, *304*, 864−867). In this study, structures and physicochemical proper-

End-on Speroxo Copper(II) Complex   Oxy-PHM

ties as well as reactivity of the copper(I) and copper(II) complexes supported by a series of tridentate ligands having the same N-[2-(2-pyridyl)ethyl]-1,5-diazacyclooctane framework have been examined in detail to shed light on the chemistry dictated in the active sites of mononuclear copper monooxygenases. The ligand exhibits unique feature to stabilize the copper(I) complexes in a T-shape geometry and the copper(II) complexes in a distorted tetrahedral geometry. Low temperature oxygenation of the copper(I) complexes generated the mononuclear copper(II) end-on superoxo complexes, the structure and spin state of which have been further characterized by density functional theory (DFT) calculations. Detailed kinetic analysis on the O$_2$-adduct formation reaction gave the kinetic and thermodynamic parameters providing mechanistic insights into the association and dissociation processes of O$_2$ to the copper complexes. The copper(II) end-on superoxo complex thus generated gradually decomposed to induce aliphatic ligand hydroxylation. Kinetic and DFT studies on the decomposition reaction have suggested that C−H bond abstraction occurs unimolecularly from the superoxo complex with subsequent rebound of the copper hydroperoxo species to generate the oxygenated product. The present results have indicated that a superoxo species having a four-coordinate distorted *tetrahedral* geometry could be reactive enough to induce the direct C−H bond activation of aliphatic substrates in the enzymatic systems.
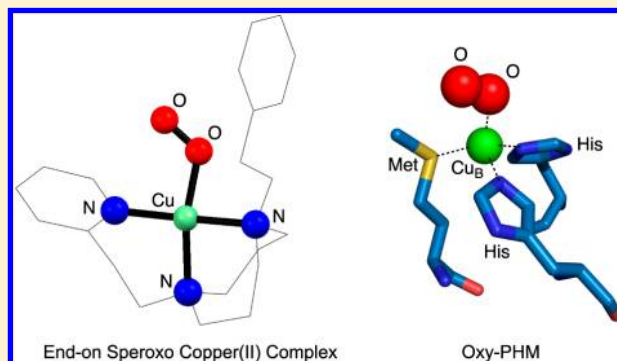
■ INTRODUCTION

Dioxygen activation at a mononuclear copper reaction center has attracted much recent attention because of its strong relevance to biological and synthetic oxidation/oxygenation reactions.[1−12] For instance, peptidylglycine α-hydroxylating monooxygenase (PHM), dopamine β-monooxygenase (DβM), and tyramine β-monooxygenase (TβM) have been reported to catalyze aliphatic C−H bond hydroxylation of their respective substrates (dopamine, peptide hormones, and tyramine, respectively) using a mononuclear copper active-oxygen species.[1,13−16] These enzymes possess a similar active site consisting of two different mononuclear copper reaction centers (designated as Cu$_A$ and Cu$_B$) separated by ∼11 Å.[17] According to the X-ray structure of resting PHM reported by

Amzel and his co-workers, Cu$_A$ site exhibits a distorted trigonal planar geometry with three histidine imidazole ligands, whereas Cu$_B$ site has a distorted tetrahedral geometry consisting with two histidine imidazole ligands, one methionine thioether ligand, and a water molecule as shown in Figure 1A.[18,19]

It has been suggested that the Cu$_A$ site is associated with electron transfer from ascorbate (physiological reductant) to the Cu$_B$ site acting as the reaction center for dioxygen activation and subsequent substrate hydroxylation. Recently, Amzel and his co-workers also determined the crystal structure of the oxy-form of PHM to demonstrate that Cu$_B$ exhibits a
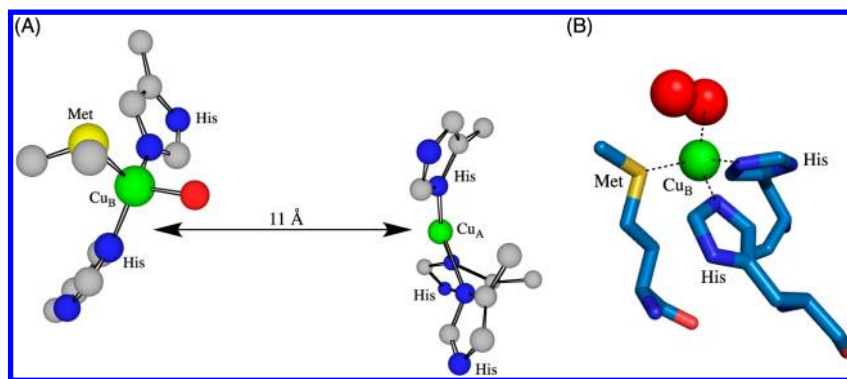
Figure 1. (A) Active site structure of PHM.[17] (B) The copper-superoxo species involved in oxy-PHM.[20].

distorted *tetrahedral* geometry including an end-on superoxo species (η^1-$O_2^{\bullet-}$) as shown in Figure 1B.[20] The recent enzymatic studies as well as the theoretical studies have suggested that the mononuclear copper(II) superoxo species (Figure 1B) could be a key reactive intermediate that is directly involved in the C−H bond activation of the substrates.[4,13,15,19,21−26] However, little is known about the physicochemical properties and reactivity of such an end-on superoxo copper(II) species having a distorted *tetrahedral* geometry.

In the synthetic modeling studies, a great deal of effort has been made to obtain insights into the structure, physicochemical properties, and reactivity of mononuclear copper(II) active-oxygen complexes.[27−42] With respect to the mononuclear copper(II)-superoxo complex, Kitajima and co-workers reported the first crystal structure of a *side-on* superoxo copper(II) complex S^S supported by a sterically demanding tridentate ligand, which exhibits a five-coordinate *square pyramidal* structure as shown in Figure 2 (left).[28] However, it
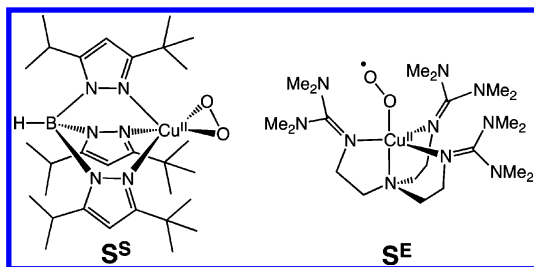

Figure 2. Structurally characterized copper(II)-superoxo complexes: $[Cu^{II}(\eta^2$-$O_2)([HB(3$-tBu$$-5-iPrpz$)_3])]^+$ (S^S)[28] and $[Cu^{II}(\eta^1$-$O_2)$-$(TMG_3tren)]^+$ (S^E).[35]

was later found that the reaction of the corresponding copper(I) complex $[Cu^I([HB(3$-tBu$$-5-iPrpz$)_3])]$ with O_2

gave a mixture of the mononuclear copper(II)-superoxo complex and a dinuclear copper(II) side-on peroxo complex, (μ-η^2:η^2-peroxo)dicopper(II), *in solution*. Thus, they re-examined the spectroscopic features of the mononuclear copper(II) side-on superoxo complex using the more sterically demanding ligand HB(3-Ad-5-iPr-pz)$_3^-$ (Ad = adamantyl) to demonstrate that the complex has a diamagnetic ground state ($S = 0$) and exhibits weak absorption bands at 383, 452, 699, and 980 nm with extinction coefficients smaller than 300 M^{-1} cm^{-1}.[29]

More recently, Schindler et al. reported a mononuclear copper(II) *end-on* superoxo complex $[Cu^{II}(\eta^1$-$O_2)$-$(TMG_3tren)]^+$ (S^E) supported by tris(tetramethylguanidino)-tren (TMG$_3$tren) tetradentate ligand (Figure 2, right).[35] In this case, the complex exhibits a five-coordinate *trigonal bipyramidal* geometry with an end-on superoxide as one of the axial ligands. The end-on superoxo complex S^E exhibits a relatively intense absorption band at 447 nm ($\varepsilon = 3400$ M^{-1} cm^{-1}) together with broad absorption bands at 680 and 780 nm. Subsequent NMR analyses and theory clearly indicated that the compound has a triplet ground state ($S = 1$).[40]

With respect to reactivity of the mononuclear copper(II) superoxo complexes, no experimental data are available for Kitajima's side-on superoxo complex, $[Cu^{II}(\eta^2$-$O_2)([HB(3$-tBu-5-iPrpz$)_3])]^+$ (S^S). In contrast, the end-on superoxo complex, $[Cu^{II}(\eta^1$-$O_2)(TMG_3tren)]^+$ (S^E), has been shown to react with hydrogen atom donors such as phenols and TEMPO-H (2,2,6,6-tetramethylpyperidine-1-hydroxide) to generate a hydroperoxo intermediate LCu^{II}OOH.[37] In this case, they observed aliphatic ligand hydroxylation of one of the methyl groups of the tetramethylguanidino substituent.[37] The same ligand hydroxylation took place, when the copper(II) complex of the same ligand was reacted with H_2O_2 in the presence of a base or the copper(I) complex was treated with PhIO.[37] However, decomposition of the superoxo complex itself did not

Scheme 1. Formation of End-on Superoxo Copper(II) Complex 2^{R}O$_2$

(Phe(X); R = -CH$_2$CH$_2$C$_6$H$_4$X (X = OMe, Me, H, Cl, NO$_2$), iPr; R = isopropyl)
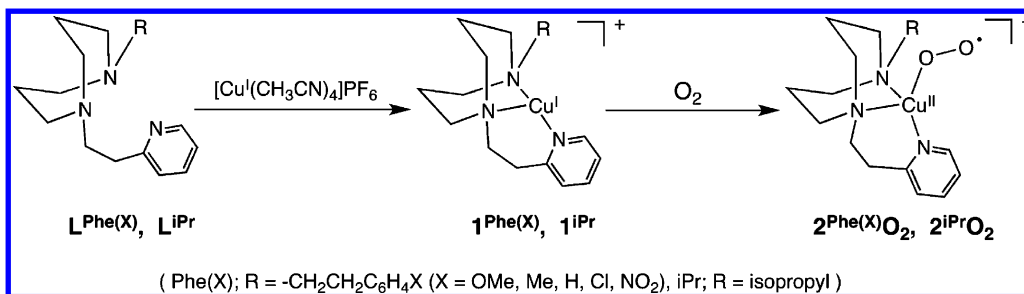
afford the hydroxylated product.[37] On the basis of these results, they concluded that the end-on superoxo complex itself was not directly involved in the aliphatic C−H bond activation, but instead a putative copper(II) oxyl radical species $LCu^{II}O^{\bullet}$ generated by O−O bond homolysis of the hydroperoxo complex $LCu^{II}OOH$ may be the real active-oxygen species.[37]

Recently, we have succeeded in developing a new type of end-on superoxo copper(II) complex $2^{Phe(X)}O_2$ having a four-coordinate distorted *tetrahedral* geometry (Scheme 1).[43] The structure of $2^{Phe(X)}O_2$ is more similar to the suggested structure of the active oxygen species of PHM (Figure 1B) as compared to Schindler's end-on superoxo complex S^E having trigonal bipyramidal structure (Figure 2).[43] The compound is generated by the reaction of copper(I) complexes supported by *tridentate* ligand $L^{Phe(X)}$ (Chart 1, X = OMe, H, NO_2) with O_2 at low temperature (Scheme 1).[43] The superoxo complex has been characterized by UV−vis [λ_{max} = 397 nm (ε = 4200 M^{-1} cm^{-1}), 570 (850), and 705 (1150)] and resonance Raman spectroscopic methods (ν_{O-O} = 1033 and ν_{Cu-O} = 457 cm^{-1}, shift to 968 and 442 cm^{-1}, respectively, upon $^{18}O_2$ substitution).[43] Moreover, the superoxo complex $2^{Phe(X)}O_2$ has been shown to have a triplet ground state (S = 1) as confirmed by electron paramagnetic resonance (EPR) and to exhibit aliphatic ligand hydroxylation reactivity.[43]

Our success may rely on the unique structural features of the supporting ligand, a *N*-[2-(2-pyridyl)ethyl]-1,5-diazacyclooctane derivative, which enforces the copper(II) complexes taking a mononuclear structure with a distorted tetrahedral geometry. So far, *N*-substituted 1,5-diazaoctane (DACO) derivative ligands have been demonstrated to provide copper(II) complexes having structural features deviating from the normal tetragonal geometry of copper(II).[38,44−48] In this study, the structure, physicochemical properties, and reactivity of the copper(I) and copper(II) complexes including the superoxo complexes 2^RO_2 supported by $L^{Phe(X)}$ and L^{iPr} (Scheme 1) have been examined in detail to shed light on the chemistry of resting states, reduced states, and oxidized states of the corresponding enzymes.

EXPERIMENTAL SECTION

Materials and Methods. The reagents and the solvents used in this study, except the ligands and the copper complexes, were commercial products of the highest available purity and were further purified by the standard methods, if necessary.[49] Ligands 1-(2-phenethyl)-5-[2-(2-pyridyl)ethyl]-1,5-diazacyclooctane ($L^{Phe(H)}$), 1-[2-(4-nitrophenyl)ethyl]-5-[2-(2-pyridyl)ethyl]-1,5-diazacyclooctane ($L^{Phe(NO2)}$), and 1-[2-(4-methoxyphenyl)ethyl]-5-[2-(2-pyridyl)ethyl]-1,5-diazacyclooctane ($L^{Phe(OMe)}$) and their copper(I) complexes ($1^{Phe(H)}$, $1^{Phe(NO2)}$, and $1^{Phe(OMe)}$) and copper(II) complexes ($2^{Phe(NO2)}Cl$ and $2^{Phe(NO2)}OAc$) were prepared according to the reported procedures.[43] FT-IR spectra were recorded on a Jasco FTIR-4100, and UV−visible spectra were taken on a Hewlett-Packard 8453 photo diode array spectrophotometer equipped with a Unisoku thermostatted cell holder USP-203 designed for low temperature measurements. ^1H NMR spectra were recorded on a JEOL LMN−ECP300WB, a JEOL ECP400, a JEOL ECS400, or a Varian UNITY INOVA 600 MHz spectrometer. ESI-MS (electrospray ionization mass spectra) measurements were performed on a PE SCIEX API 150EX, a PerSeptive Biosystems Mariner Biospectrometry workstation, or a Micromass LCT spectrometer. Elemental analyses were performed on a Perkin-Elmer or a Fisons instruments EA1108 Elemental Analyzer.

Dioxygen concentrations in organic solvents (acetone, tetrahydrofuran (THF), and propionitrile) at various temperatures (−70 ∼ −90 °C) were calculated by using the equation, $C_T = C_0 \, (d_T/d_0)$, where C_T and d_T are the O_2 concentration and the density of solution

at temperature T, and C_0 and d_0 are the known values at room temperature.[50] Because of the small solubility of O_2 in liquids, the density of the solution can be assumed equal to that of pure solvent. For several common solvents, densities were experimentally determined in a wide range of temperatures and fit satisfactorily with the following equation, $d_T = a - bT$ (T in K; the parameters a and b are found in the literatures).[51]

1-[2-(4-Methylphenyl)ethyl]-1,5-diazacyclooctane. A mixture of DACO (1,5-diazacyclooctane)·2HBr (7.0 g, 25 mmol) and KOH (2.8 g, 50 mmol) in CH_3CN-H_2O (5: 1, 120 mL) was stirred for 1 h at room temperature. Then, 2-(4-methylphenyl)ethyl bromide (5.0 g, 25 mmol) and triethylamine (13 g, 100 mmol) were added to the solution, and the resulting solution was refluxed for 14 h. The solvent was removed under reduced pressure, and the resulting residue was dissolved in water (10 mL), to which NaOH(aq) was added slowly until the pH of the solution became 14. The aqueous solution was extracted with $CHCl_3$ (20 mL × 3), and the combined organic layer was dried over Na_2SO_4. After removal of Na_2SO_4 by filtration, evaporation of the solvent gave dark brown oil. Purification by Kugelrohr distillation (200 °C, 5.0 Torr) afforded the pure product as a colorless oil in a 19% isolated yield. ^1H NMR ($CDCl_3$, 300 MHz) δ 1.61 (4 H, pentet, J = 5.7 Hz, $-CH_2-$), 2.31 (3 H, s, $-CH_3$), 2.57−2.71 (8 H, m, $-CH_2-$), 2.84 (4 H, t, J = 5.7 Hz, $-CH_2-$), 7.09 (4 H, br s, ArH); HRMS (FAB$^+$) m/z = 232.1933, calcd for $C_{15}H_{24}N_2$ = 232.1940.

1-[2-(4-Methylphenyl)ethyl]-5-[2-(2-pyridyl)ethyl]-1,5-diazacyclooctane ($L^{Phe(Me)}$). To a methanol solution (40 mL) containing 1-[2-(4-methylphenyl)ethyl]-1,5-diazacyclooctane (680 mg, 3.1 mmol) and 2-vinylpyridine (1.5 g, 15.5 mmol) was added acetic acid (1.0 g, 15.5 mmol), and the mixture was refluxed for 1 day. Removal of the solvent by evaporation gave brown oil, from which ligand $L^{Phe(Me)}$ was isolated by alumina column chromatography (eluent: AcOEt) in 56%. ^1H NMR ($CDCl_3$, 300 MHz) δ = 1.65 (4 H, pentet, J = 5.7 Hz, $-CH_2-$), 2.31 (3 H, s, $-CH_3$), 2.72−2.79 (12 H, m, $-CH_2-$), 2.93 (4 H, s, $-CH_2-$), 7.09−7.19 (6 H, m, ArH), 7.57 (1 H, dt, J = 1.8 Hz and J = 7.5 Hz, PyH_4), 8.52 (1 H, d, J = 4.8 Hz, PyH_6); HRMS (FAB$^+$) m/z = 338.2603, calcd for $C_{22}H_{32}N_3$ = 338.2596.

1-[2-(4-Chlorophenyl)ethyl]-1,5-diazacyclooctane. This compound was prepared by a similar procedure as described for the synthesis of 1-[2-(4-methylphenyl)ethyl]-1,5-diazacyclooctane using 2-(4-chlorophenyl)ethyl bromide instead of (2-(4-methylphenyl)ethyl) bromide in a 14% isolated yield. ^1H NMR ($CDCl_3$, 300 MHz) δ = 1.61 (4 H, pentet, J = 5.7 Hz, $-CH_2-$), 2.63−2.76 (8 H, m, $-CH_2-$), 2.84 (4 H, t, J = 5.7 Hz, $-CH_2-$), 7.12 (2 H, d, J = 8.4 Hz, ArH), 7.25 (2 H, d, J = 8.4 Hz, ArH); HRMS (FAB$^+$) m/z = 253.1474, calcd for $C_{14}H_{22}N_2Cl_1$ = 253.1472.

1-[2-(4-Chlorophenyl)ethyl]-5-[2-(2-pyridyl)ethyl]-1,5-diazacyclooctane ($L^{Phe(Cl)}$). This compound was prepared by a similar procedure as described for the synthesis of $L^{Phe(Me)}$ using 1-[2-(4-chlorophenyl)ethyl]-1,5-diazacyclooctane instead of 1-[2-(4-methylphenyl)ethyl]-1,5-diazacyclooctane in 65%. ^1H NMR ($CDCl_3$, 300 MHz) δ = 1.64 (4 H, pentet, J = 5.7 Hz, $-CH_2-$), 2.71−2.77 (12 H, m), 2.92 (4 H, s), 7.07−7.26 (6 H, m, ArH), 7.58 (1 H, td, J = 1.6 Hz and J = 7.5 Hz, PyH_4), 8.52 (1 H, d, J = 4.2 Hz, PyH_6); HRMS (FAB$^+$) m/z = 357.1972, calcd for $C_{21}H_{28}Cl_1N_3$ = 357.1975.

1-Isopropyl-5-[2-(2-pyridyl)ethyl]-1,5-diazacyclooctane (L^{iPr}). 1-Isopropyl-1,5-diazacyclooctane was prepared according to the reported procedures.[52] To a methanol solution (20 mL) containing 1-isopropyl-1,5-diazacyclooctane (0.33 g, 2.1 mmol) and 2-vinilpyridine (0.67 g, 6.3 mmol) was added acetic acid (0.38 g, 6.3 mmol), and the mixture was refluxed for 2 days. The solvent was removed by evaporation, and the resulting residue was dissolved in water (15 mL), to which NaOH(aq) was added slowly until the pH of the solution became 14. The aqueous solution was extracted with CH_2Cl_2 (20 mL × 5), and the combined organic layer was dried over Na_2SO_4. After removal of Na_2SO_4 by filtration, the solvent was evaporated to give a brown oil, from which L^{iPr} was isolated by alumina column chromatography (eluent: from AcOEt:hexane = 1: 1 to AcOEt only) in 77%. ^1H NMR ($CDCl_3$, 600 MHz) δ = 0.98 (6 H, d, J = 6.8 Hz), 1.65 (4 H, pentet, J = 6.0 Hz), 2.74 (4 H, t, J = 6.0 Hz), 2.84 (4 H, t, J

9467

dx.doi.org/10.1021/ic301272h | *Inorg. Chem.* 2012, 51, 9465−9480

= 6.0 Hz), 3.00 (4 H, m), 3.12 (1 H, septet, J = 6.8 Hz), 7.10 (1 H, ddd, J = 7.6, 5.0, and 1.1 Hz), 7.19 (1 H, br d, J = 7.6 Hz), 7.58 (1 H, td, J = 7.6 and 1.1 Hz), 8.52 (1 H, ddd, J = 5.0, 1.9, and 0.9 Hz); HRMS (FAB, pos): m/z = 262.2274. Calcd for $C_{16}H_{28}N_3$ 262.2283.

Since all the copper(I) complexes are sensitive to air, all the manipulations for the syntheses, crystallization, and stock solution preparations of copper(I) complexes were carried out under Ar atmosphere in a glovebox (Miwa DBO-1KP, $[O_2]$ < 1 ppm).

$[Cu^I(L^{Phe(Me)})](PF_6)$ ($1^{Phe(Me)}$). Ligand $L^{Phe(Me)}$ (67.4 mg, 0.2 mmol) was treated with an equimolar amount of $[Cu^I(CH_3CN)_4]PF_6$ (74.0 mg, 0.2 mmol) in CH_2Cl_2–CH_3CN (7: 1, 4 mL). After stirring the mixture for 5 min at room temperature, insoluble material was removed by filtration. Addition of ether (100 mL) to the filtrate gave a pale yellow powder that was precipitated by standing the mixture for several minutes. The supernatant was then removed by decantation, and the remained pale yellow solid was washed with ether three times (50 mL × 3) and dried to give complex $1^{Phe(Me)}$ in 62%. Single crystals of $1^{Phe(Me)}$ were obtained by vapor diffusion of ether into a CH_2Cl_2–CH_3CN (10 : 1) solution of the complex. FT-IR (KBr) 840 cm^{-1} (PF_6^-); HRMS (FAB$^+$): m/z 400.1813, calcd for $C_{22}H_{31}CuN_3$ 400.1814; Anal. Calcd for $[Cu^I(L^{Phe(Me)})]PF_6 \cdot H_2O$ ($C_{22}H_{33}CuF_6N_3O_1P_1$): C, 46.85; H, 5.90; N, 7.45. Found: C, 46.64; H, 5.50; N, 7.77.

$[Cu^I(L^{Phe(Cl)})](PF_6)$ ($1^{Phe(Cl)}$). This compound was prepared by a similar procedure as described for the synthesis of $1^{Phe(Me)}$ in 51% using $L^{Phe(Cl)}$ instead of $L^{Phe(Me)}$. Single crystals of $1^{Phe(Cl)}$ were obtained by diffusion of n-hexane into a CH_2Cl_2–CH_3CN (10 : 1) solution of the complex. FT-IR (KBr) 840 cm^{-1} (PF_6^-); HRMS (FAB$^+$): m/z 420.1279, calcd for $C_{21}H_{28}CuN_3Cl_1$ 420.1267; Anal. Calcd for $[Cu^I(L^{Phe(Cl)})]PF_6 \cdot H_2O$ ($C_{21}H_{28}CuF_6N_3Cl_1P_1$): C, 44.63; H, 4.99; N, 7.39. Found: C, 44.53; H, 4.98; N, 7.42.

$[Cu^I(L^{iPr})](PF_6)$ (1^{iPr}). To an acetonitrile solution (30 mL) containing L^{iPr} (50 mg, 0.19 mmol) was added $[Cu^I(CH_3CN)_4]PF_6$ (71 mg, 0.19 mmol), when the color of the solution turned light yellow. After stirring 5 min, the volume of the solvent was reduced under reduced pressure, and diethyl ether (5 mL) was added to the residue to give a light yellow powder of the product (69 mg, 76%). Single crystal was obtained by vapor diffusion of ether into a CH_3CN solution of the complex. FT-IR (KBr) 842 cm^{-1} (PF_6^-); ESI-MS (pos) m/z = 324.2 calcd for: $C_{16}H_{27}BCuN_6$: 324.2; Anal. Calcd for $[Cu^I(L^{iPr})]PF_6 \cdot 0.05[Cu(CH_3CN)_4]PF_6$ ($C_{16.4}H_{27.6}Cu_{1.05}F_{6.3}N_{3.2}P_{1.05}$): C, 40.32; H, 5.69; N, 9.17. Found: C, 40.28; H, 5.40; N, 8.96.

$[Cu^{II}(L^{Phe(NO2)})(NO_2)](BF_4)$ ($2^{Phe(NO2)}NO_2$). Ligand $L^{Phe(NO2)}$ (50 mg, 0.14 mmol) was treated with an equimolar amount of $Cu^{II}SO_4 \cdot 5H_2O$ (34 mg, 0.14 mmol) in CH_3OH (20 mL). After stirring the mixture for 3 min at room temperature. $NaNO_2$ (12 mg, 0.18 mmol) and NH_4BF_4 (42 mg, 0.40 mmol) were added to the solution continuously. Insoluble material was then removed by filtration. Addition of ether (100 mL) to the filtrate gave a blue powder that was precipitated by standing the mixture for several minutes. The supernatant was then removed by decantation, and the remaining blue solid was washed with ether three times and dried to give the complex in 87%. Single crystals of $2^{Phe(NO2)}NO_2$ were obtained by vapor diffusion of n-hexane into CH_2Cl_2 solution of the complex. FT-IR (KBr) 1053 cm^{-1} (BF_4^-); Anal. Calcd for $[Cu^{II}(L^{Phe(NO2)})(NO_2)](BF_4) \cdot H_2O$ ($C_{22}H_{32}BCuF_4N_5O_5$): C, 43.27; H, 5.19; N, 12.02. found: C, 43.54; H, 5.16; N, 12.08.

$[Cu^{II}(L^{iPr})(OAc)](BF_4)$ ($2^{iPr}OAc$). To an ethanol solution (30 mL) containing L^{iPr} (59 mg, 0.22 mmol) was added $Cu(OAc)_2 \cdot H_2O$ (45 mg, 0.22 mmol), when the color of the solution turned dark blue. After stirring 5 min, NH_4BF_4 (70 mg, 0.67 mmol) was added to the solution, and the mixture was stirred for 2 min. The volume of the solvent was reduced under reduced pressure to give a blue powder, which was collected by filtration and dried (73 mg, 69%). Single crystals were obtained by vapor diffusion of ether into an acetone solution of the complex. FT-IR (KBr) 1608 cm^{-1} (C=O), 1055 cm^{-1} (BF_4^-); Anal. Calcd for: $[Cu^{II}(L^{iPr})(OAc)]BF_4 \cdot 0.5H_2O$ ($C_{18}H_{31}BCuF_4N_3O_{2.5}$): C, 45.06; H, 6.51; N, 8.76; Found: C, 45.01; H, 6.21; N, 8.95; ESI-MS (pos) m/z = 382.8 calcd for: $C_{18}H_{30}CuN_3O_2$: 383.2.

$[Cu^{II}(L^{iPr})(N_3)](BF_4)$ ($2^{iPr}N_3$). To a methanol solution (30 mL) containing L^{iPr} (50 mg, 0.19 mmol) was added $CuSO_4 \cdot 5H_2O$ (48 mg, 0.19 mmol), when the color of the solution turned dark blue. After stirring for 5 min, NaN_3 (16 mg, 0.25 mmol) was added to give a green solution. After stirring for 2 min, NH_4BF_4 (70 mg, 0.67 mmol) was added to the solution, and the mixture was stirred for additional 2 min. Volume of the solvent was reduced under reduced pressure to give dark green powder, which was collected by filtration and dried (69 mg, 80%). Single crystals were obtained by vapor diffusion of ether into an acetone solution of the complex. FT-IR (KBr) 2037 cm^{-1} (N_3^-), 1057 cm^{-1} (BF_4^-); Anal. Calcd for: $[Cu^{II}(L^{iPr})(N_3)]BF_4$ ($C_{16}H_{27}BCuF_4N_6$): C, 42.35; H, 6.00; N, 18.52. Found: C, 42.29; H, 5.74; N, 18.25; ESI-MS (pos) m/z = 324.2 calcd for: $C_{16}H_{27}CuN_3$: 324.2.

$[Cu^{II}(L^{iPr})(Cl)](PF_6)$ ($2^{iPr}Cl$). To an ethanol solution (50 mL) containing L^{iPr} (70 mg, 0.27 mmol) was added $CuCl_2$ (36 mg, 0.27 mmol), when the color of the solution turned greenish blue. After stirring for 5 min, NH_4PF_6 (130 mg, 0.81 mmol) was added to the solution, and the mixture was stirred for additional 2 min. The volume of the solvent was reduced under reduced pressure to give a green powder, which was collected by filtration and dried (96 mg, 71%). FT-IR (KBr) 841 cm^{-1} (PF_6^-); Anal. Calcd for: $[Cu^{II}(L^{iPr})Cl]PF_6 \cdot 0.5H_2O$ ($C_{16}H_{28}ClCuF_6N_3O_{0.5}P$): C, 37.36; H, 5.49; N, 8.17; Found: C, 37.65; H, 5.32; N, 7.85; ESI-MS (pos) m/z = 359.1 calcd for: $C_{16}H_{27}ClCuN_3$: 359.1. Single crystals of $2^{iPr}Cl$ were obtained as a BPh_4 salt $[Cu^{II}(L^{iPr})(Cl)](BPh_4)$ by adding $NaBPh_4$ into a CH_3CN solution of the PF_6 salt $[Cu^{II}(L^{iPr})(Cl)](PF_6)$ obtained above.

$[Cu^{II}(L^{iPr})(NO_2)](BF_4)$ ($2^{iPr}NO_2$). This compound was prepared as a blue powder by a similar procedure described for the synthesis of $2^{iPr}N_3$ by using $NaNO_2$ instead of NaN_3 (79%). Single crystals were obtained by vapor diffusion of ether into an acetone solution of the complex. FT-IR (KBr) 1046 cm^{-1} (BF_4^-), Anal. Calcd for: $[Cu^{II}LNO_3]PF_6 \cdot 0.4H_2O$ ($C_{16}H_{27.8}BCuF_4N_4O_{2.4}$): C, 41.33; H, 6.03; N, 12.05. Found: C, 41.56; H, 5.83; N, 11.78; ESI-MS (pos) m/z = 324.2 calcd for: $C_{16}H_{27}CuN_3$: 324.2.

X-ray Structure Determination. Each single crystal obtained was mounted on a loop with mineral oil, and all X-ray data were collected on a Rigaku R-AXIS RAPID diffractometer using filtered Mo-$K\alpha$ radiation. The structures were solved by direct methods (SIR 2008[53]) and expanded using Fourier techniques. The non-hydrogen atoms were refined anisotropically by full-matrix least-squares on F^2. The hydrogen atoms were attached at idealized positions on carbon atoms and were not refined. All structures in the final stages of refinement showed no movement in the atom positions. The calculations were performed using Single-Crystal Structure Analysis Software, version 3.8 (Rigaku Corporation: The Woodlands, TX, 2000−2006). Crystallographic parameters are summarized in Table 1. Atomic coordinates, thermal parameters, and intramolecular bond distances and angles are deposited in the Supporting Information (CIF file format).

EPR Measurements. EPR spectra of copper(II) complexes were recorded on a JEOL X-band spectrometer (JES-RE1XE) with an attached variable temperature apparatus. The EPR spectra were measured in frozen acetone at 77 K. The magnitude of modulation was chosen to optimize the resolution and the signal-to-noise (S/N) ratio of the observed spectra under nonsaturating microwave conditions. The g values and the hyperfine coupling constants were calibrated with a Mn^{2+} marker.

Kinetic Measurements. Kinetic measurements for the oxygenation reaction of copper(I) complexes, $1^{Phe(X)}$ (X = OMe, Me, H, Cl, NO$_2$) and 1^{iPr}, and the decomposition reaction of the generated copper(II) superoxo complexes, $2^{Phe(X)}O_2$ and $2^{iPr}O_2$, were performed using a Hewlett-Packard 8453 photo diode array spectrophotometer with a Unisoku thermostatted cell holder designed for low temperature measurements (USP-203, a desired temperature can be fixed within ±0.5 °C) in an appropriate solvent (3 mL) at low temperature. For the oxygenation reaction of the copper(I) complexes, O$_2$ gas was rapidly introduced to a solution of the copper(I) complex in a UV cell (1.0 cm path length) through a silicon rubber cap by using a gastight syringe, and the increase of the absorption band due to the superoxo complex

Table 1. X-ray Crystallographic Data of Copper(I) Complexes $1^{Phe(Me)}$ and 1^{iPr}

	$1^{Phe(Me)}$	1^{iPr}
formula	$C_{22}H_{31}N_3CuPF_6$	$C_{16}H_{27}N_3CuPF_6$
formula weight	546.02	469.92
crystal system	monoclinic	orthorhombic
space group	$P2_1/c$ (#14)	$Pbca$ (#61)
a, Å	7.805(9)	10.6388(4)
b, Å	19.739(17)	13.7319(5)
c, Å	15.504(17)	26.100(1)
α, deg	90	90
β, deg	94.66(5)	90
γ, deg	90	90
V, Å^3	2381(4)	3813.0(3)
Z	4	8
$F(000)$	1128.00	1936.00
D_{calcd}, g/cm^{-3}	1.523	1.637
T, K	153	103
crystal size, mm	$0.40 \times 0.30 \times 0.20$	$0.20 \times 0.10 \times 0.10$
μ (Mo$K\alpha$), cm^{-1}	10.468	12.921
$2\theta_{max}$, deg	54.9	55.0
no. of reflns measd	21644	34770
no. of reflns obsd	5402 (all reflections)	4364 (all reflections)
no. of variables	329	244
$R1^a$	0.0487	0.0261
$wR2^b$	0.0761	0.0588
GOF	1.003	1.008

$^aR1 = \sum ||F_o| - |F_c|| / \sum |F_o|$. $^bwR2 = [\sum w(F_o^2 - F_c^2)^2 / \sum w(F_o^2)^2]^{1/2}$

was monitored. The pseudo-first-order rate constants for the formation and decomposition of the copper(II) superoxo complexes were determined from the plots of $\ln(\Delta A)$ vs time based on the time course of the absorption change at λ_{max} due to the copper(II) superoxo complexes.

Ligand Hydroxylation Reaction. Typically, $1^{Phe(H)}$ (10.6 mg, 0.02 mmol) was dissolved into deaerated acetone (10 mL) under anaerobic conditions at room temperature, and then the solution was cooled to −80 °C and kept under O$_2$ atmosphere for 24 h. A mixture of the hydroxylated ligand and the original ligand was obtained after an ordinary workup treatment of the reaction mixture with NH$_4$OHaq and following extraction by CH$_2$Cl$_2$. The yield of hydroxylated ligand was determined as 34% based on the copper(I) starting material by using an integral ratio in the ^{1}H NMR spectrum between the benzylic proton (-CH-OH-) at δ = 4.63 (dd, J = 3.5 and 7.1 Hz) of the hydroxylated ligand and the pyridine protons at the 6-position (δ = 8.55) from both the hydroxylated ligand and the original ligand. HRMS (FAB, pos) m/z = 340.2389, calcd for $C_{21}H_{30}ON_3$ 340.2389. The yields of ligand hydroxylation of other ligands $L^{Phe(X)}$ were determined similarly by ^{1}H NMR as 33, 32, 31, and 29% for X = OMe, Me, Cl, and NO$_2$, respectively; the benzylic proton (-CH-OH-) for the hydroxylated ligand: δ = 4.59 (dd, J = 3.5 and 7.5 Hz) for X = OMe; δ = 4.57 (dd, J = 3.5 and 7.1 Hz) for X = Me; δ = 4.60 (dd, J = 3.5 and 7.0 Hz) for X = Cl; δ = 4.75 (dd, J = 3.5 and 7.1 Hz) for X = NO$_2$.

Computational Methods. All geometries were fully optimized at the M11-L[54] level of density functional theory (DFT) using the Stuttgart [8s7p6d | 6s5p3d] ECP10MWB contracted pseudopotential basis set on Cu[55] and the 6-31G(d) basis set[56] on all other atoms. In addition, 3 uncontracted f functions having exponents 5.100, 1.275, and 0.320 were placed on Cu. The grid = ultrafine option in Gaussian 09[57] (which was used for all calculations, see ref (1) in Supporting Information for full citation of ref 56) was chosen for integral evaluation and an automatically generated density-fitting basis set was used within the resolution-of-the-identity approximation for the evaluation of Coulomb integrals. The nature of all stationary points was verified by analytic computation of vibrational frequencies, which were also used for the computation of zero-point vibrational energies,

molecular partition functions (with all frequencies below 50 cm^{-1} replaced by 50 cm^{-1} when computing free energies), and for determining the reactants and products associated with each transition-state structure (by following the normal modes associated with imaginary frequencies). Partition functions were used in the computation of 298 K thermal contributions to free energy employing the usual ideal-gas, rigid-rotator, harmonic oscillator approximation.[58] Solvation effects associated with acetone as solvent were accounted for by using the SMD continuum solvation model.[59] Free energy contributions were added to single-point M11-L electronic energies computed with the SDD basis set on Cu and the 6-311+G(2df,p) basis set on all other atoms to arrive at final, composite free energies.

Addition of triplet molecular oxygen to the closed shell singlet Cu(I) complexes may in principle generate either open shell singlet or triplet products. These species were characterized by weak coupling between two different spin centers, and the singlet states were thus not well described by a single determinant as is implicit in the standard Kohn−Sham density functional formalism. In such instances, Kohn−Sham DFT is not directly applicable,[58,60−62] and we adopt the Yamaguchi broken-spin-symmetry (BS) procedure[63,64] to compute the energy of the spin-purified low-spin (LS) state as

$$^{LS}E = \frac{^{BS}E\left(^{HS}\langle S^2 \rangle - {}^{LS}\langle S^2 \rangle\right) - {}^{HS}E\left(^{BS}\langle S^2 \rangle - {}^{LS}\langle S^2 \rangle\right)}{^{HS}\langle S^2 \rangle - {}^{BS}\langle S^2 \rangle}$$

where HS refers to the single-determinantal high-spin coupled state that is related to the low-spin state by spin flip(s) and $\langle S^2 \rangle$ is the expectation value of the total spin operator applied to the appropriate determinant. This broken-symmetry DFT approach has routinely proven effective for the prediction of state-energy splittings in metal coordination compounds.[65−68] Time-dependent DFT (TDDFT) calculations were performed to predict the UV/visible electronic excitations of postulated intermediates. The B3LYP[69] density functional, the Stuttgart [8s7p6d | 6s5p3d] ECP10MWB contracted pseudopotential basis set on Cu, and the 6-311+G(d) basis set[56] on all other atoms were used for the TDDFT calculations with G09 default nonequilibrium solvation effects computed using the SMD continuum solvation model for acetonitrile or acetone as solvent.[70]

■ RESULTS AND DISCUSSION

Synthesis and Characterization. *Copper(I) Complexes.* The tridentate ligands $L^{Phe(X)}$ (X = OMe, Me, H, Cl, NO$_2$) were prepared by Michael addition of 1-(2-p-substituted-phenethyl)-1,5-diazacyclooctane to 2-vinylpyridine in refluxing methanol in the presence of excess amount of acetic acid.[71] Ligand L^{iPr} was prepared in a similar manner by using 1-isopropyl-1,5-diazacyclooctane instead of the p-substituted phenetyl derivative as indicated in Scheme 2.

Scheme 2. Synthesis of Supporting Ligands L^R
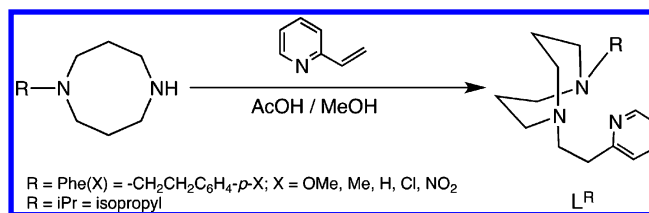
Treatment of the ligand with $[Cu^I(CH_3CN)_4](PF_6)$ in CH$_3$CN−CH$_2$Cl$_2$ under anaerobic conditions gave the corresponding mononuclear copper(I) complex, $1^{Phe(X)}$ and 1^{iPr}. The crystal structures of $1^{Phe(OMe)}$, $1^{Phe(H)}$, and $1^{Phe(NO2)}$ have already been reported in our previous communication,[43] and those of $1^{Phe(Me)}$, $1^{Phe(Cl)}$, and 1^{iPr} have been determined in this study as shown in Figure 3 ($1^{Phe(Me)}$ and 1^{iPr}) and Supporting Information, Figure S1 ($1^{Phe(Cl)}$). The crystallo-
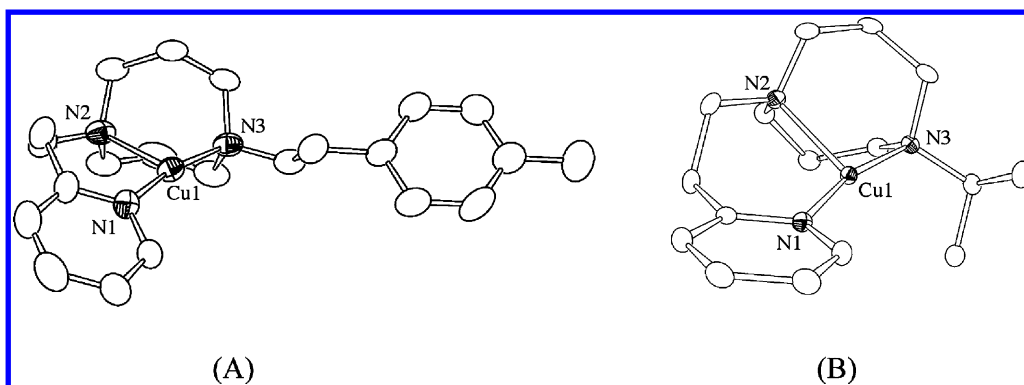
Figure 3. ORTEP drawings of (A) $1^{Phe(Me)}$ and (B) 1^{iPr} showing 50% probability thermal ellipsoids. The counteranion and the hydrogen atoms are omitted for clarity.

Table 2. Selected Bond Lengths (Å) and Angles (deg) of $1^{Phe(Me)}$ and 1^{iPr}

	$1^{Phe(Me)}$		
Cu(1)−N(1)	1.899(3)	Cu(1)−N(2)	2.184(4)
Cu(1)−N(3)	1.968(4)		
N(1)−Cu(1)−N(2)	101.30(14)	N(1)−Cu(1)−N(3)	168.27(14)
N(2)−Cu(1)−N(3)	90.33(14)		
	1^{iPr}		
Cu(1)−N(1)	1.9080(14)	Cu(1)−N(2)	2.1783(13)
Cu(1)−N(3)	1.9865(14)		
N(1)−Cu(1)−N(2)	103.15(6)	N(1)−Cu(1)−N(3)	165.82(6)
N(2)−Cu(1)−N(3)	90.62(5)		

graphic data and the selected bond lengths and angles are summarized in Tables 1 and 2 for $1^{Phe(Me)}$ and 1^{iPr} and Supporting Information, Tables S1 and S2 for $1^{Phe(Cl)}$, respectively.

All the copper(I) complexes $1^{Phe(X)}$ (X = OMe, Me, H, Cl, and NO$_2$) and 1^{iPr} exhibit a similar three-coordinate T-shape structure ligated by the three nitrogen atoms N(1), N(2), and N(3) of the supporting ligand.[43] The sum of the three angles around the copper center [∠N(1)−Cu(1)−N(2), ∠N(1)−Cu(1)−N(3), and ∠N(2)−Cu(1)−N(3)] is equal to 360°, indicating that the copper ion and the three nitrogen atoms exist in the same plane. It should be noted that the copper(I) complexes do *not* involve a CH$_3$CN molecule as an external coligand even though the complexes were prepared using [Cu^I(CH$_3$CN)$_4$]$^+$ as the metal source and were crystallized in a CH$_3$CN-containing solvent (see Experimental Section). In general, copper(I) complexes with an ordinary didentate or tridentate ligand do involve one or more CH$_3$CN external coligand(s) so as to take on a favorable tetrahedral geometry (assuming that they are prepared in a CH$_3$CN-containing solvent system). Consistent with experiment, our DFT calculations at the M11-L level of theory predict that the free energy of binding of CH$_3$CN to the $1^{Phe(H)}$ system proceeds with an unfavorable free energy change of +4.9 kcal/mol at 25 °C.

Such a weak binding ability of the copper(I) complexes 1^R toward external substrate was also seen in the treatment with CO, which is a well-known substrate exhibiting strong binding to ordinary copper(I) complexes. For instance, little spectral changes were observed upon addition of CO gas to an acetone solution of 1^R at 25 °C, even though CO can form an adduct at very low temperature (−85 °C) as shown in Supporting Information, Figure S2. The calculated free energy change for CO binding to $1^{Phe(H)}$ was found to be −4.2 kcal/mol assuming

standard state conditions (e.g., 1 M CO solution). However, at 25 °C the concentration of CO in acetone will be much less than this value, thereby disfavoring binding. At low temperatures, decreased entropic influence and greater CO solubility lead to complexation. Thus, it could be said that our ligands L^R highly stabilizes copper(I) complexes with the three-coordinate T-shape structure without any external coligand. This structural feature of the copper(I) complexes is somewhat different from that of the Cu$_B$ site of reduced PHM, where the copper(I) center exhibits a distorted four-coordinate tetrahedral geometry with H$_2$O or CO as the external coligand.[18,72]

Copper(II) Complexes. A series of copper(II) complexes having a different counteranion (Y) have been prepared to examine the structural features of the copper(II) complexes supported by the ligand L^R. The crystal structures of $2^{Phe(NO2)}Cl$ and $2^{Phe(NO2)}OAc$ supported by $L^{Phe(NO2)}$ have already been reported in our previous Communication,[43] and that of $2^{Phe(NO2)}NO_2$ has been determined in the present study (see Supporting Information, Figure S3, Table S3 and S4). The copper(II) complexes of the isopropyl ligand L^{iPr} ($2^{iPr}Cl$, $2^{iPr}OAc$, $2^{iPr}N_3$, and $2^{iPr}NO_2$) have also been determined in this study (Figure 4), and the crystallographic data and the selected bond lengths and angles are summarized in Tables 3 and 4, respectively. All the copper(II) complexes exhibit a mononuclear structure having the counteranion as an external coligand.

The structure of the metal center of $2^{iPr}Cl$ is essentially the same with that of $2^{Phe(NO2)}Cl$,[43] having a highly distorted tetrahedral geometry with the N$_3$Cl donor set (Figure 4A). The τ_4 values for $2^{iPr}Cl$ and $2^{Phe(NO2)}Cl$, a simple geometry index for four-coordinate complexes proposed by Houser and his co-workers, are 0.57 and 0.54, respectively; $\tau_4 = [360° − (\alpha + \beta)]/141$, where α and β are the two largest θ angles in the four-coordinate species.[73] The values of τ_4 will range from 1.00 for a

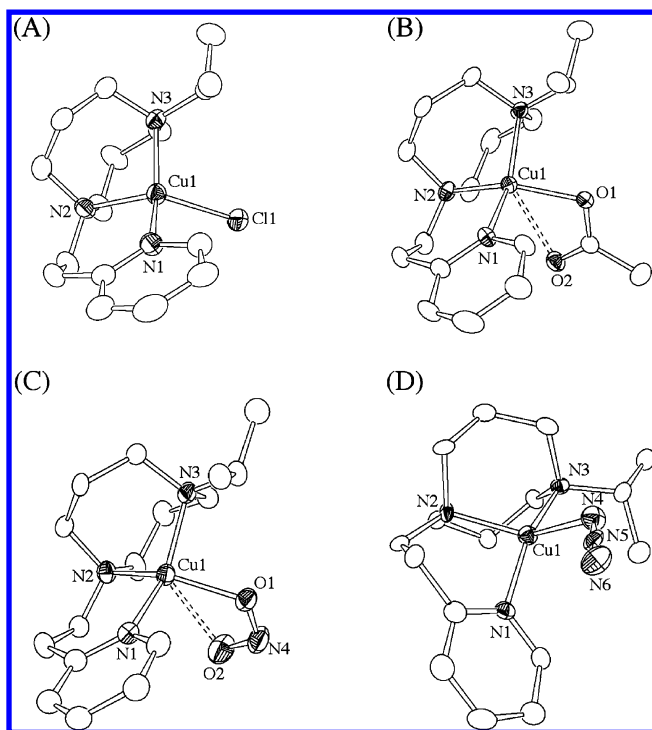**Figure 4.** ORTEP drawings of (A) $2^{iPr}Cl$, (B) $2^{iPr}OAc$, (C) $2^{iPr}NO_2$, and (D) $2^{iPr}N_3$ showing 50% probability thermal ellipsoids. The uncoordinated counteranion and the hydrogen atoms are omitted for clarity.

perfect tetrahedral geometry to zero for a perfect square planar geometry.[73] The isopropyl (iPr) and the phenetyl (Phe(X))

substituents may prevent formation of a Cu_2Cl_2 (doubly chloride-bridged) dimer.

The acetate complex $2^{iPr}OAc$ also shows a monomeric structure as in the case of $2^{Phe(NO2)}OAc$, in which the acetate anion looks like it acts as a didentate ligand. However, the distance of Cu−O(2) ($d_{Cu-O(2)}$ = 2.588(3) Å) is significantly larger than that of Cu−O(1) ($d_{Cu-O(1)}$ = 1.973(3) Å) (Table 4). Thus, the structure of $2^{iPr}OAc$ can be regarded as a distorted tetrahedron with the N_3O donor set having a weakly interacting acetate O(2) atom (so-called capped tetrahedron), where the τ_4 value is 0.45.

Recently, Amzel and co-workers reported the crystal structures of PHM soaked with $NaNO_2$ and NaN_3.[74] They unambiguously demonstrated that only the Cu_B site of PHM can bind NO_2^- and N_3^- anions, consistent with the conclusion that Cu_B is the oxygen- and substrate-binding site whereas Cu_A is the electron acceptor site from ascorbate.[17,20] In this study, the crystal structures of our model compounds $2^{iPr}NO_2$ ($2^{Phe(NO2)}NO_2$) and $2^{iPr}N_3$ were compared to those of the active sites of the resting state of PHM having NO_2^- and N_3^- coordinating counteranion.

The overall structure of $2^{iPr}NO_2$ is similar to that of $2^{iPr}OAc$ (Figure 4B), where the distance of Cu−O(1) ($d_{Cu-O(1)}$ = 2.009(3) Å) is much shorter than that of Cu−O(2) ($d_{Cu-O(2)}$ = 2.513(4) Å) (Figure 4C and Table 4). Thus, the structure of $2^{iPr}NO_2$ can also be described as distorted tetrahedron with a weakly interacting O(2) atom (capped tetrahedron). $2^{Phe(NO2)}NO_2$ exhibits a similar structure to that of $2^{iPr}NO_2$; $d_{Cu-O(1)}$ = 2.018(4) Å and $d_{Cu-O(2)}$ = 2.432(4) Å; (Supporting Information, Figure S3). The binding of NO_2^- in the Cu_B site of the nitrite-soaked PHM (copper-to-nitrite oxygen distances are 1.9 and 2.6 Å) is comparable to those of our model compounds.[74]

Table 3. X-ray Crystallographic Data of Copper(II) Complexes $2^{iPr}Y$

	$2^{iPr}Cl$	$2^{iPr}OAc$	$2^{iPr}NO_2$	$2^{iPr}N_3$
formula	$C_{40}H_{47}BClCuN_3$	$C_{18}H_{30}BCuF_4N_3O_2$	$C_{16}H_{27}BCuF_4N_4O_2$	$C_{16}H_{27}BCuF_4N_6$
formula weight	679.64	470.80	457.76	453.78
crystal system	triclinic	monoclinic	orthorhombic	monoclinic
space group	$P\bar{1}$ (#2)	$P2_1/n$ (#14)	$P2_12_12$ (#18)	Pn (#7)
a, Å	11.1894(5)	11.9825(5)	9.7137(6)	7.4111(5)
b, Å	11.3597(6)	12.6970(5)	26.834(2)	14.733(1)
c, Å	14.2362(8)	14.8164(6)	7.4613(5)	9.2356(6)
α, deg	103.344(1)	90	90	90
β, deg	90.250(1)	109.849(2)	90	98.941(1)
γ, deg	102.542(1)	90	90	90
V, Å^3	1715.8(2)	2120.3(1)	1944.8(3)	996.2(1)
Z	2	4	4	2
$F(000)$	718.00	980.00	948.00	470.00
D_{calcd}, g/cm^{-3}	1.315	1.475	1.563	1.513
T, K	113	113	103	113
crystal size, mm	0.32 × 0.16 × 0.03	0.52 × 0.28 × 0.09	0.10 × 0.10 × 0.10	0.24 × 0.21 × 0.06
μ (MoKa), cm^{-1}	7.474	10.833	11.800	11.467
$2\theta_{max}$, deg	54.9	54.9	54.9	54.9
no. of reflns measd	16970	20291	18830	9544
no. of reflns obsd	7975 [$I > 1.00\sigma(I)$]	4039 [$I > 1.00\sigma(I)$]	4450 (all reflections)	7450 [$I > 1.00\sigma(I)$]
no. of variables	460	310	280	281
$R1^a$	0.0504	0.0566	0.0538	0.0454
$wR2^b$	0.1239	0.1871	0.1330	0.0732
GOF	0.997	0.978	1.163	1.047

$^aR1 = \sum||F_o| - |F_c||/\sum|F_o|$. $^bwR2 = [\sum w(F_o^2 - F_c^2)^2/\sum w(F_o^2)^2]^{1/2}$.

Table 4. Selected Bond Lengths (Å) and Angles (deg) of Copper(II) Complexes 2^{iPr}Y

2^{iPr}Cl

Cu(1)−N(1)	1.976(4)	Cu(1)−N(2)	1.996(4)
Cu(1)−N(3)	2.036(4)	Cu(1)−Cl(1)	2.2345(11)
Cl(1)−Cu(1)−N(1)	96.54(10)	Cl(1)−Cu(1)−N(2)	131.36(11)
Cl(1)−Cu(1)−N(3)	99.45(10)	N(1)−Cu(1)−N(2)	98.87(16)
N(1)−Cu(1)−N(3)	148.55(14)	N(2)−Cu(1)−N(3)	90.61(15)

2^{iPr}OAc

Cu(1)−N(1)	2.022(4)	Cu(1)−N(2)	2.000(4)
Cu(1)−N(3)	2.036(3)	Cu(1)−O(1)	1.973(3)
Cu(1)−O(2)	2.588(3)		
O(1)−Cu(1)−N(1)	92.17(12)	O(1)−Cu(1)−N(2)	148.12(13)
O(2)−Cu(1)−N(3)	95.45(11)	O(1)−Cu(1)−O(2)	56.29(10)
N(1)−Cu(1)−N(2)	98.78(14)	N(1)−Cu(1)−N(3)	148.54(14)
N(2)−Cu(1)−N(3)	90.65(13)		

2^{iPr}NO$_2$

Cu(1)−N(1)	2.025(4)	Cu(1)−N(2)	1.980(4)
Cu(1)−N(3)	2.042(3)	Cu(1)−O(1)	2.009(3)
Cu(1)−O(2)	2.513(4)		
O(1)−Cu(1)−N(1)	92.10(13)	O(1)−Cu(1)−N(2)	149.66(14)
O(2)−Cu(1)−N(3)	95.41(13)	O(1)−Cu(1)−O(2)	54.32(12)
N(1)−Cu(1)−N(2)	98.77(14)	N(1)−Cu(1)−N(3)	147.19(14)
N(2)−Cu(1)−N(3)	90.64(13)		

2^{iPr}N$_3$

Cu(1)−N(1)	1.979(3)	Cu(1)−N(2)	2.024(3)
Cu(1)−N(3)	2.016(3)	Cu(1)−N(4)	1.983(4)
N(4)−Cu(1)−N(1)	91.85(12)	N(4)−Cu(1)−N(2)	141.73(11)
N(4)−Cu(1)−N(3)	94.80(12)	N(1)−Cu(1)−N(2)	95.66(12)
N(1)−Cu(1)−N(3)	158.38(11)	N(2)−Cu(1)−N(3)	91.79(11)

Table 5. UV−vis Data, EPR Parameters, and Redox Potentials of Copper(II) Complexes 2^{iPr}Y

complex	λ_{max} (nm)^a ε (M^{-1} cm^{-1})	EPR parameter^b		$E_{1/2}$ (V)^c	ΔE_p (V)
2^{iPr}Cl	643 (260)	$g_{\parallel}$ = 2.22	$A_{\parallel}$ = 144 G	0.015	0.11
	854 (300)	$g_{\perp}$ = 2.09			
2^{iPr}OAc	655 (310)	$g_{\parallel}$ = 2.23	$A_{\parallel}$ = 156 G	−0.22	0.14
	745 (300)	$g_{\perp}$ = 2.06			
2^{iPr}NO$_2$	650 (340)	$g_{\parallel}$ = 2.22	$A_{\parallel}$ = 160 G	−0.07	0.12
	725 (350)	$g_{\perp}$ = 2.08			
2^{iPr}N$_3$	435 (2220)	$g_{\parallel}$ = 2.22	$A_{\parallel}$ = 153 G	−0.03	0.15
	643 (690)	$g_{\perp}$ = 2.09			
	∼780 (shoulder)				

^{a}In CH$_3$CN. ^{b}In acetone. ^{c}In CH$_3$CN containing 0.1 M tetra-*n*-butylammonium perchlorate (TBAP) at 25 °C. Working electrode glassy carbon, counter electrode Pt, reference electrode Ag/0.01 M AgNO$_3$, scan rate 50 mV/s.

The azide complex **2^{iPr}N$_3$** also exhibits a mononuclear structure with a highly distorted *tetrahedral* geometry having a monodentate N$_3^-$ ligand; $d_{Cu-N(4)}$ = 1.983(4) Å, τ_4 = 0.42 (Figure 4D). The structural feature of **2^{iPr}N$_3$** is also similar to that of the Cu$_B$ site in the NaN$_3$-soaked PHM; four-coordinate tetrahedral geometry with $d_{Cu-N(4)}$ = 2.0 Å.[74] All these results suggest that the copper(II) complexes supported by **L^{iPr}** and **L$^{Phe(X)}$** are good structure models for the Cu$_B$ site of PHM having the copper(II) oxidation state.

To obtain information about the copper(II) complexes in solution, UV−vis and EPR spectra as well as cyclic voltammetry of **2^{iPr}Y** were measured as summarized in Table 5. The spectra and cyclic voltammograms are presented in Supporting Information (Supporting Information, Figure S4 ∼ S15).

The copper(II) complexes exhibit at least two broad and weak d-d bands around 650 nm and above 700 nm (the d-d bands of **2^{iPr}Cl** are exceptionally well separated, see Supporting Information, Figure S4), and **2^{iPr}N$_3$** shows a distinct LMCT band due to the azide ligand at 435 nm (Supporting Information, Figure S7). To explore the electronic-structures in detail, time-dependent DFT (TD-DFT) calculations employing the hybrid B3LYP density functional and accounting for nonequilibrium solvation were undertaken. The calculated spectra and the predicted λ_{max} values for the **2^{iPr}Y** complexes were found to be in good agreement with the experimental UV−vis data and are listed in the Supporting Information along with the description of molecular orbitals involved in the individual excitations (Supporting Information, Figures S16−S19 and Tables S5−S8). Analysis of the TD-B3LYP excitations reveals a complex pattern for the broad peaks in the 600−800 nm range whereas the LMCT bands at higher energies could be easily assigned as in the case of **2^{iPr}N$_3$**. All of the excitations take place into the same acceptor orbital, which is the lowest unoccupied molecular orbital (LUMO) in the beta manifold, but the individual occupied orbitals from which the excitations occur are diverse as illustrated in the Supporting Information,

Tables S5−S8. The LUMOs exhibit significant Cu d character with smaller contributions from π^* orbitals of nitrogen atoms of 2^{iPr} and coordinating atoms of the anionic ligands. For the electronic excitations in the 600−800 nm range, the individual occupied orbitals from which the excitations occur display significant amplitude on Cu centers (and to a lesser amount on 2^{iPr} ligands) as well as on the π^* orbitals of the coordinated anionic ligands. On the other hand, the peaks in the 400−430 nm range for the $2^{iPr}N_3$ involve electronic excitations from molecular orbitals with mainly N_3-π^* character to LUMO orbitals confirming the LMCT assignment.

The EPR spectra of the copper(II) complexes are presented in Supporting Information, Figures S8∼S11, and the EPR parameters are summarized in Table 5. The complexes exhibit relatively small $g_\parallel$ (∼2.22) and $A_\parallel$ values as compared to those of ordinary copper(II) complexes having tetragonal geometry, suggesting that the *tetrahedral* distortion of the four-coordinate structure is maintained in solution.

Kitajima and co-workers reported a mononuclear copper(II)-chloride complex supported by $HB(3,5-iPr_2pz)_3$ [hydrotris(3,5-diisopropyl-1-pyrazolyl)borate] having a tetrahedral geometry.[75] This compound was, however, easily converted to a five-coordinate copper(II)-Cl complex having additional dimethyl-formamide (DMF) or dimethylsulfoxide (DMSO) solvent molecules, when the four-coordinate copper(II)-Cl complex was treated with a small amount of DMF or DMSO.[75] With our copper(II)-chloride complex $2^{iPr}Cl$, on the other hand, no spectral change was observed even in the presence of large excess (5.0 M) of coordinating solvent such as DMF, DMSO, and CH_3CN. Thus, the four-coordinate copper(II) complex $2^{iPr}Cl$ strongly resists the binding of external fifth ligand. In other words, the copper(II) complexes supported by ligand L^R strongly favor the four-coordinate structure.

The copper(II) complexes $2^{iPr}Y$ exhibited a quasi-reversible Cu^{II}/Cu^{I} redox couple ($E_{1/2}$) around 0 V vs Ag/0.01 M $AgNO_3$ in CH_3CN. The slight difference in $E_{1/2}$ among the complexes may be due to the different electronic effects of the coordinating counteranions **Y**.

Formation and Characterization of Copper(II) Super-oxo Complex. *Reversible O_2-Binding to Copper(I) Complex.* As we have already reported in the previous Communication, the copper(I) complexes supported by the phenetyl derivative $L^{Phe(H)}$ reacted with O_2 in a 1:1 ratio (determined by manometry) at a low temperature (−85 °C) to produce copper(II) superoxo complexes $2^{Phe(H)}O_2$, exhibiting characteristic absorption bands at 397 nm (ε = 4200 M^{-1} cm^{-1}), 570 nm (850), and 705 nm (1150) (Scheme 1).[43] In this study, essentially the same spectra were obtained in the reactions of other phenetyl derivatives $1^{Phe(X)}$ (X = OMe, Me, Cl, and NO_2) and isopropyl derivative 1^{iPr} with O_2 under the same experimental conditions, demonstrating that the same copper-(II)-superoxo complexes $2^{Phe(X)}O_2$ (X = OMe, Me, Cl, and NO_2) and $2^{iPr}O_2$ were generated in all the ligand systems. A typical example of the UV−vis spectral change for the oxygenation reaction of 1^{iPr} is shown in Figure 5, where an intense LMCT band at 395 nm (ε = 5810 M^{-1} cm^{-1}) readily appeared together with the broad absorption bands around 585 (980) and 723 nm (1240).

In the resonance Raman spectrum excited at λ_{ex} = 406.7 nm, the superoxo complex $2^{Phe(H)}O_2$ exhibited O−O and Cu−O stretching vibrations at 1033 cm^{-1} and 457 cm^{-1}, respectively, which shifted to 968 cm^{-1} and 442 cm^{-1} upon $^{18}O_2$-substitution.[43] Although the difference spectrum between the
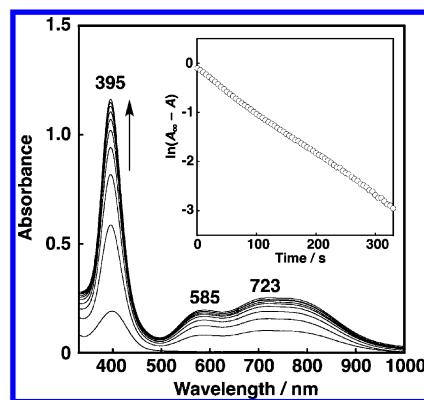

Figure 5. UV−vis spectral change for the oxygenation reaction of 1^{iPr} (0.2 mM) in acetone at −85 °C (50 s interval). Inset: First-order plot based on the absorption changes at 395 nm.

$^{16}O_2$ and $^{18}O_2$ derivatives clearly indicated the existence of the O−O stretching vibration band, its intensity was significantly weaker as compared to the Cu−O band.[43] In this study, we have re-examined the resonance Raman spectrum of the superoxo copper(II) species using $2^{iPr}O_2$ (isopropyl derivative) using different excitation laser light at λ_{ex} = 442 and 647 nm. However, no improvement of the peak intensity was obtained for the O−O stretching vibration band. The O−O moiety of the end-on superoxide ligand may take some different geometries relative to the ligand (L^{iPr}) backbone, causing the broadening of the Raman peak due to O−O stretching.

The fine-structure EPR study indicated that $2^{Phe(H)}O_2$ has a spin triplet ground state (S = 1).[43] This assignment is supported by DFT calculations. Theoretical calculations at the M11-L level of theory show that both end-on and pseudo-side-on geometries are possible for $2^{Phe(H)}O_2$ species, with the former isomer being slightly (∼0.6 kcal/mol) more stable than the latter. For both isomers, the triplet spin state was found to be the ground state with the singlet structures higher in energy by about 7.0 kcal/mol (Supporting Information, Figure S25).

The formation of $2^{iPr}O_2$ shown in Figure 5 follows first-order kinetics in the presence of an excess amount of O_2 (9.26 mM in acetone at −85 °C; O_2 concentrations were determined as described in Experimental Section), and the pseudo-first-order rate constant k_{obs} was determined from the first-order plot shown in the inset of Figure 5. Then, the rate-dependence on the O_2-concentration was examined as shown in Figure 6,
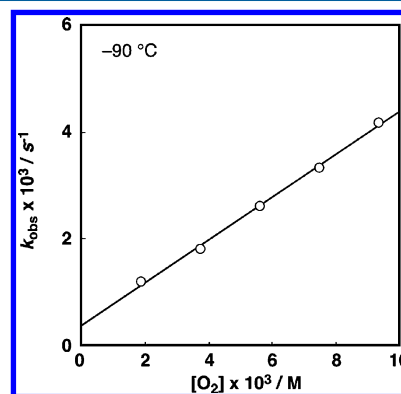

Figure 6. Dependence of the observed first-order rate constant (k_{obs}) on the dioxygen concentration for the formation of $2^{iPr}O_2$ in acetone at −90 °C.
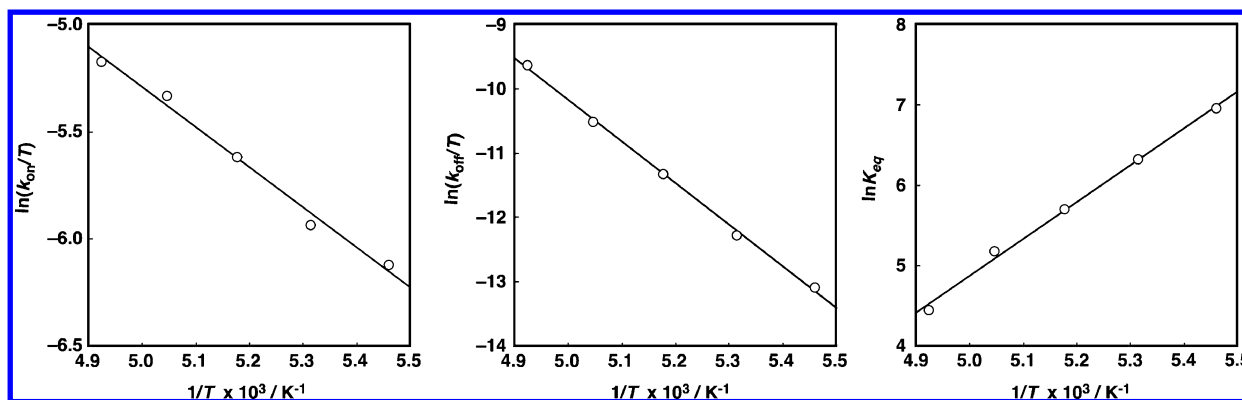
Figure 7. Plots of $\ln(k_{on}/T)$, $\ln(k_{off}/T)$, and $\ln K_{eq}$ vs $1/T$ for the reaction of $\mathbf{1^{iPr}}$ and O_2 to give $\mathbf{2^{iPr}O_2}$ in acetone.

Table 6. Kinetic and Thermodynamic Parameters for the Formation of Copper(II)-Superoxo Complexes (1:1-Adduct) upon Low Temperature Oxygenation of Copper(I) Complexes

ligand	solvent	k_{on} (M^{-1} s^{-1})[a]	activation parameters (k_{on})[b]	k_{off} (s^{-1})[a]	activation parameters (k_{off})[b]	K_{eq} (M^{-1})[a]	thermodynamic parameters (K_{eq})[b]
L^{iPr}	acetone	$(4.0 \pm 0.1) \times 10^{-1}$	$\Delta H^{\ddagger} = 15.5 \pm 0.9$ $\Delta S^{\ddagger} = -164 \pm 5$	$(3.8 \pm 0.7) \times 10^{-4}$	$\Delta H^{\ddagger} = 53.5 \pm 1.2$ $\Delta S^{\ddagger} = -14.4 \pm 6.2$	$(1.05 \pm 0.1) \times 10^{3}$	$\Delta H^{0} = -38.0 \pm 1.3$ $\Delta S^{0} = -150 \pm 7$
L^{iPr}	THF	$(7.6 \pm 0.2) \times 10^{-1}$	$\Delta H^{\ddagger} = 24.4 \pm 1.3$ $\Delta S^{\ddagger} = -110 \pm 7$	$(1.1 \pm 0.1) \times 10^{-3}$	$\Delta H^{\ddagger} = 33.9 \pm 1.1$ $\Delta S^{\ddagger} = -13 \pm 6$	$(7.04 \pm 0.1) \times 10^{2}$	$\Delta H^{0} = -9.50 \pm 0.31$ $\Delta S^{0} = 2.57 \pm 1.60$
tmpa[77]	EtCN	$(1.18 \pm 0.01) \times 10^{4}$	$\Delta H^{\ddagger} = 31.6 \pm 0.5$ $\Delta S^{\ddagger} = 10 \pm 3$	$(1.59 \pm 0.01) \times 10^{1}$	$\Delta H^{\ddagger} = 61.5 \pm 0.5$ $\Delta S^{\ddagger} = 18 \pm 3$	$(7.42 \pm 0.04) \times 10^{2}$	$\Delta H^{0} = -29.8 \pm 0.2$ $\Delta S^{0} = -108 \pm 1$
Me$_6$tren[77]	EtCN	$(9.5 \pm 0.4) \times 10^{4}$	$\Delta H^{\ddagger} = 17.1 \pm 0.6$ $\Delta S^{\ddagger} = -52 \pm 3$	$(7.0 \pm 0.3) \times 10^{-2}$	$\Delta H^{\ddagger} = 62.0 \pm 0.6$ $\Delta S^{\ddagger} = 76 \pm 3$	$(1.35 \pm 0.04) \times 10^{6}$	$\Delta H^{0} = -44.9 \pm 0.2$ $\Delta S^{0} = -128 \pm 1$

[a]At −90 °C. [b]Units: $\Delta H^{\ddagger}$ and ΔH^{0} in kJ mol^{-1} $\Delta S^{\ddagger}$ and ΔS^{0} in J K^{-1} mol^{-1}.

where the plot of k_{obs} against [O$_2$] gave a linear correlation with a distinct intercept on the y-axis (Figure 6 shows the rate-dependence on [O$_2$] at −90 °C. The rate dependence on [O$_2$] at −85, −80, −75, and −70 °C are shown in Supporting Information, Figure S20). Existence of such an intercept in the plot indicates that the O$_2$-binding is reversible (eq 1),

$$\mathbf{1^{iPr}} + O_2 \underset{k_{off}}{\overset{k_{on}}{\rightleftarrows}} \mathbf{2^{iPr}O_2} \tag{1}$$

and the association rate constant k_{on} and the dissociation rate constant k_{off} of O$_2$ are equal to the slope and the intercept, respectively (eq 2).[76]

$$k_{obs} = k_{on}[O_2] + k_{off} \tag{2}$$

Reversibility of the O$_2$-binding has been confirmed by the separate experiments demonstrating that O$_2$ was removed by bubbling with Ar and applying a vacuum and then reforming the superoxo complex by exposure to O$_2$ (Supporting Information, Figure S21). Then, the equilibrium constant K_{eq} can be determined by eq 3,

$$K_{eq} = k_{on}/k_{off} \tag{3}$$

and the kinetic and thermodynamic parameters were determined from the linear plots of $\ln(k_{on}/T)$, $\ln(k_{off}/T)$, and $\ln K_{eq}$ against $1/T$ as presented in Figures 7, respectively. The kinetic and thermodynamic parameters for the reactions in THF were determined in the similar manner (Supporting Information, Figures S22 and S23), and data are listed in Table 6 together with those of the reactions of $\mathbf{1^{iPr}}$ in acetone. The kinetic and thermodynamic parameters for the (1: 1) O$_2$-adduct formation reactions between the copper(I) complexes supported by the tripodal tetradentate ligands tmpa [tris(2-

pyrydylmethyl)amine] and the Me$_6$tren [tris(2-dimethylaminoethyl)amine] in propionitrile reported by Schindler, Zuberbühler, and co-workers are also included in Table 6.[77] Similar results for the tmpa system were also reported by Karlin, Zuberbühler, and co-workers.[78] However, the O$_2$-adduct formation reaction of $\mathbf{1^{iPr}}$ in propionitrile was too slow, competing with the self-decomposition reaction of generated superoxo complex $\mathbf{2^{iPr}O_2}$. Thus, the O$_2$-binding process of $\mathbf{1^{iPr}}$ in propionitrile could not be examined accurately.

The association of O$_2$ to $\mathbf{1^{iPr}}$ (k_{on} process) in both acetone and THF are significantly slower than those of the copper(I) complexes of tmpa and Me$_6$tren in propionitrile. In the tmpa and Me$_6$tren ligand systems, it was suggested that the solvent molecule EtCN binds strongly to the copper(I) ion and thus dissociation of EtCN from the copper(I) complex is rate-limiting for the O$_2$-adduct formation (dissociative mechanism). This is reflected in the positive or small negative $\Delta S^{\ddagger}$ values for tmpa and Me$_6$tren systems, respectively (Table 6). On the other hand, our ligand system (L^{iPr}) exhibits very large negative $\Delta S^{\ddagger}$ values both in acetone and THF, suggesting that the association of O$_2$ to the copper(I) ion is rate-limiting (associative mechanism), and the transition-state structure of the O$_2$-adduct is highly restricted (Table 6). This is the reason for the much smaller k_{on} values in the L^{iPr} ligand system.

With respect to the k_{off} process, the positive $\Delta S^{\ddagger}$ values in the tmpa and Me$_6$tren systems suggest that dissociation of O$_2$ from the superoxo complex is rate-limiting and the resulting copper(I) complex quickly binds to EtCN. This may be due to the stronger binding of the nitrile solvent to copper(I). On the other hand, the negative $\Delta S^{\ddagger}$ values in the L^{iPr} system indicate that association of the solvent molecules (acetone and THF) to

copper(I) complexes is rate-limiting rather than O_2-dissociation.

With regard to the thermodynamic parameters, the L^{iPr} system in THF is exceptional, showing a small negative ΔH^0 and positive ΔS^0. This clearly indicates that the binding energy of end-on superoxide to copper(II) ion in $2^{iPr}O_2$ is weaker as compared with those in the other systems. This may be due to the existence of some interaction between a THF molecule and the superoxo complex $2^{iPr}O_2$. On the other hand, the thermodynamic parameters in acetone are similar to those of tmpa and Me_6tren ligand systems, where there may be no solvent coordination to the five-coordinate cupric ion in the superoxo copper(II) complexes. This may indicate that there is no solvent coordination to the copper(II) ion in $2^{iPr}O_2$ in acetone neither. The stability of the four-coordinate structure in the copper(II) oxidation state in the present ligand system has been well demonstrated above.

Reactivity of Copper(II) Superoxo Complexes. *Aliphatic Ligand Hydroxylation.* The copper(II) superoxo complex $2^{Phe(H)}O_2$ has previously been shown to undergo an aliphatic ligand hydroxylation at its benzylic position to give alkoxo-copper(II) complexes $3^{Phe(H)}$ (Scheme 3).[43] Isotope

Scheme 3. Aliphatic Ligand Hydroxylation in End-on Superoxo Copper(II) Complexes $2^{Phe(X)}O_2$

$2^{Phe(X)}O_2$ (X = OMe, Me, H, Cl, NO$_2$) $3^{Phe(X)}$
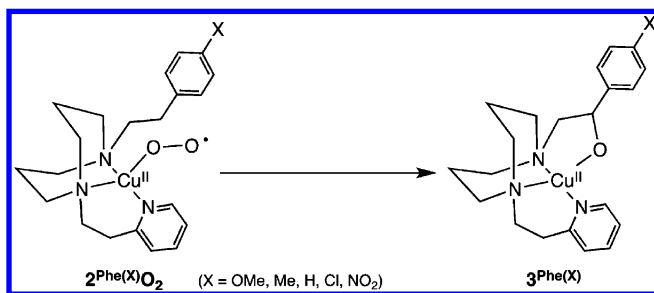
labeling experiments using $^{18}O_2$ unambiguously indicated that the oxygen atom of the hydroxyl group comes from molecular oxygen used for the preparation of $2^{Phe(H)}O_2$.[43] The ^1H NMR analysis of organic product obtained by demetalation from the final product complex using $NH_4OH(aq)$ demonstrated that the phenetyl side arm was hydroxylated in ∼35% yield based on the starting material.[43]

In this study, the decomposition (aliphatic ligand hydroxylation) process has been examined in more detail to get mechanistic insight into the C−H bond activation process (Scheme 3). Figure 8 shows the spectral change for the decomposition reaction of $2^{Phe(H)}O_2$ at −65 °C as a typical example. As clearly shown in the inset of Figure 8, the reaction obeyed first-order kinetics, suggesting that the ligand hydroxylation reaction is a unimolecular (intramolecular) process. The first-order kinetics was further confirmed by the fact that identical first-order rate constants were obtained in the copper concentration range of 0.1−0.4 mM. The decomposition reactions of all other ligands L^R also exhibited the first-order kinetics. In the reaction of perdeuterated phenetyl derivative $L^{Phe(H)}$-d_4 (ethylene linker moiety is fully deuterated) appreciable amount of kinetic isotope effect (KIE) value [KIE = 4.1; $k_{dec(H)} = 2.5 \times 10^{-4}$ s^{-1} and $k_{dec(D)} = 0.60 \times 10^{-4}$ s^{-1}] was obtained, indicating that the reaction involves the benzylic C−H bond activation. Furthermore, analysis of the rate-dependence on the reaction temperature (Eyring plot, Supporting Information, Figure S24) gives activation parameters for the
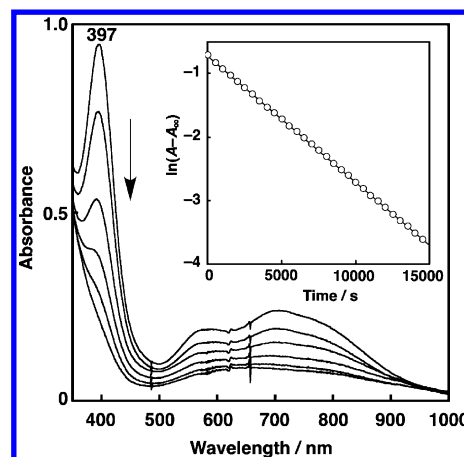
Figure 8. UV−vis spectral change for the decomposition (ligand hydroxylation) of $2^{Phe(H)}O_2$ (0.2 mM) in acetone at −65 °C. Inset: First-order plot based on the absorption changes at 395 nm.

ligand hydroxylation process as $\Delta H^{\ddagger} = 19 \pm 0.1$ kJ mol^{-1} and $\Delta S^{\ddagger} = -223 \pm 0.6$ J K^{-1} mol^{-1}.

Electronic effects of the *p*-substituent (X) on the hydroxylation reaction were also examined using a series of *p*-substituted phenetyl derivatives $2^{Phe(X)}O_2$ (X = OMe, Me, H, Cl, NO$_2$). The plot of log k_{dec} against the Hammett σ_p constants gave a negative small ρ value (−0.63; R = 0.88; Figure 9), suggesting that the reactive species exhibits a weakly
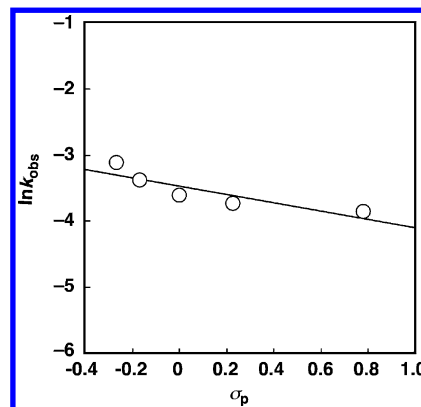
Figure 9. Hammett plot for the ligand hydroxylation in acetone at −60 °C.

nucleophilic nature and that the ligand hydroxylation reaction involves hydrogen atom abstraction from the benzylic position of the ligand side arm.

To provide microscopic insight into the details of the mechanistic pathway and various potential intermediates of the ligand hydroxylation, DFT calculations at the M11-L level of theory were undertaken (see Computational Methods section for full details). To begin, $1^{Phe(H)}$ and O_2 were chosen as the reactants, and all free energy changes in the proposed mechanisms are reported with respect to separated $1^{Phe(H)}$ and O_2 (Figure 10).

The proposed mechanism for the ligand hydroxylation starts with the formation of $2^{Phe(H)}O_2$ which can be viewed as a copper(II) superoxo complex based on the extent of localized spin density on the copper and oxygen centers. Two conformers, namely, end-on and pseudo side-on (Figure 11a and 11b, respectively), were located for $2^{Phe(H)}O_2$ that are close
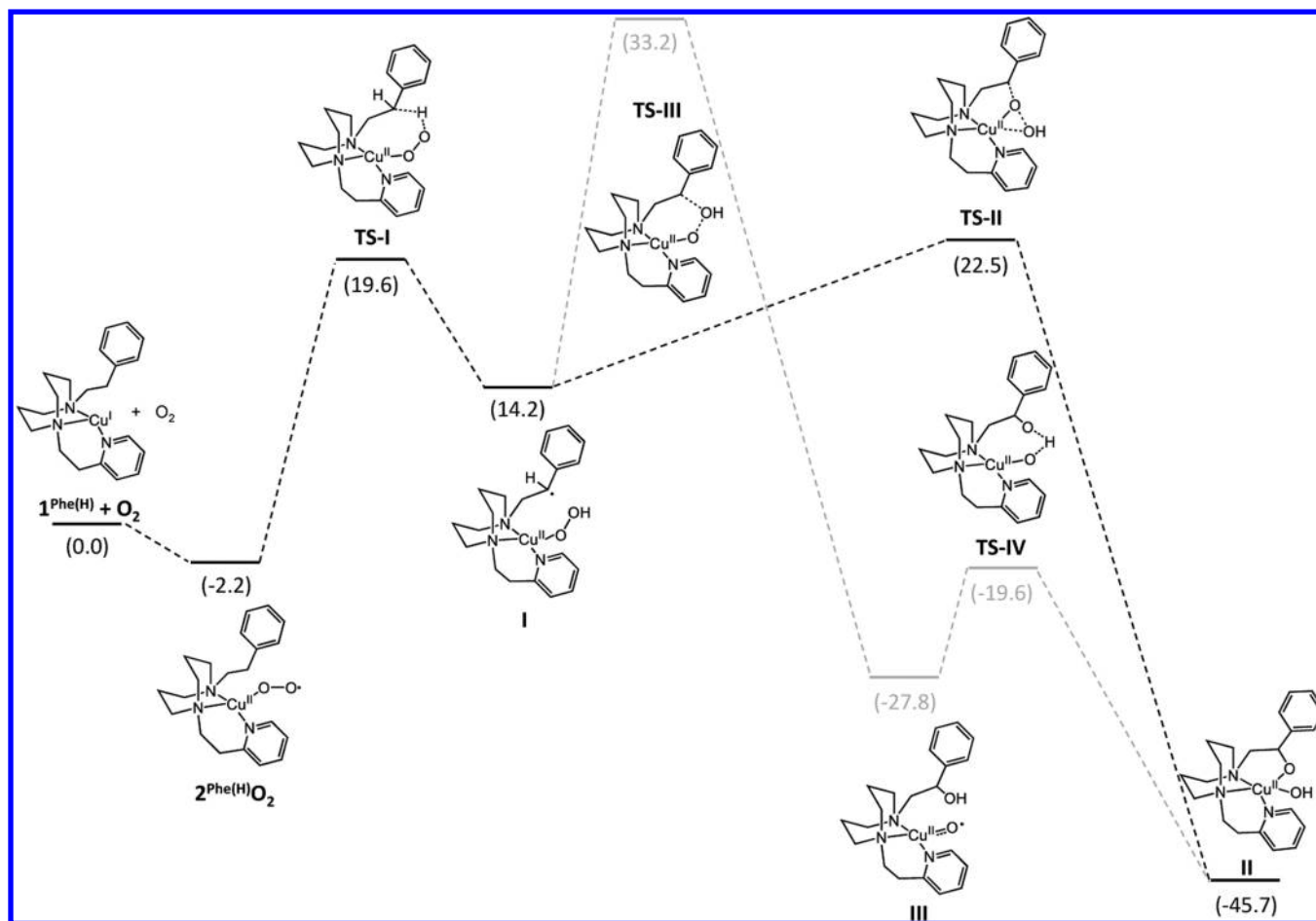
Figure 10. Proposed mechanism for the hydroxylation reaction of $1^{Phe(H)}$. Relative free energies at 298.15 K are reported in units of kcal/mol.

in energy, with the end-on structure being slightly more stable (~0.6 kcal/mol). For both conformers the triplet spin state was found to be the ground state with broken symmetry singlet structures lying about 7.0 kcal/mol higher in energy as stated above.

As a next step, we considered hydrogen atom abstraction from the benzylic position by the copper(II) superoxo unit and we located a transition state structure, **TS-I** (Figure 11c), which has a free energy of activation of 21.8 kcal/mol including tunneling effects.[79] The resulting intermediate, **I** (Figure 11d), features a copper(II) hydroperoxo complex with a nearby radical center at the benzylic position. Following generation of intermediate **I**, we have identified two possible pathways for the hydroxylation step. Path 1 involves the oxygenation of the benzylic position by the proximal oxygen to the copper center with concomitant O−O bond scission. The located transition state structure on this path, **TS-II** (Figure 11e), has $\Delta G^{\ddagger} = 8.3$ kcal/mol relative to the preceding intermediate and generates the final product, **II** (Figure 11f). This step is highly exergonic with a free energy change of −59.9 kcal/mol. Path 2 starts with the hydroxylation of the benzylic position by the hydroxo unit of the copper(II) hydroperoxo intermediate **I** also with concomitant O−O bond scission. The free energy of activation associated with the relevant transition state (TS) structure, **TS-III** (Figure 11g), is 19.0 kcal/mol relative to **I** and the resulting product, **III** (Figure 11h), with hydroxylated benzylic position and a copper(II) oxyl group is 42.0 kcal/mol more stable than **I**. In the final step of this path, the copper(II) oxyl group in

intermediate **III** abstracts the hydrogen atom of the hydroxyl group at the benzylic position, **TS-IV** (Figure11i) and generates the same final product **II** as in the first path. This step proceeds with a $\Delta G^{\ddagger}$ of 8.2 kcal/mol relative to **III**. A comparison of the free energy changes indicates that Path 1 is favored significantly over Path 2 as the rate determining step (**TS-II**) in Path 1 has a $\Delta G^{\ddagger}$ of 22.5 kcal/mol compared to 33.2 kcal/mol (**TS-III**) for Path 2, all taken relative to separated reactants. Both pathways lead to the same intermediate **II** which has a triplet ground state and can be described as a supported Cu(II) center with an additional unpaired electron delocalized over the two oxygen atoms. Subsequent reduction of intermediate **II** by unreacted copper(I) complex $1^{Phe(H)}$ and hydroxide transfer leads to the formation of the Cu(II)-alkoxide product $3^{Phe(H)}$ and Cu(II)-hydroxide byproduct, which is quite exergonic with a predicted free energy change of −35.7 kcal/mol (Scheme 4). Invocation of this comproportionation step implies a maximum yield for ligand hydroxylation of 50%. As the redox step follows the rate determining H-atom abstraction step, the second-order character of the redox step does not affect the kinetics.

In addition to these considerations of the reactions of the mononuclear complex, we also investigated the possible formation and reactivity of dinuclear species. Our calculations indicate that the formation of dinuclear *trans*-peroxo ($4^{Phe(H)}$ *trans*-peroxo; this compound has a geometry that is actually intermediate between side-on and end-on peroxo, see Supporting Information, Figure S25) and bis-μ-oxo ($4^{Phe(H)}$ bis-μ-oxo) species are possible with standard-state ΔG values
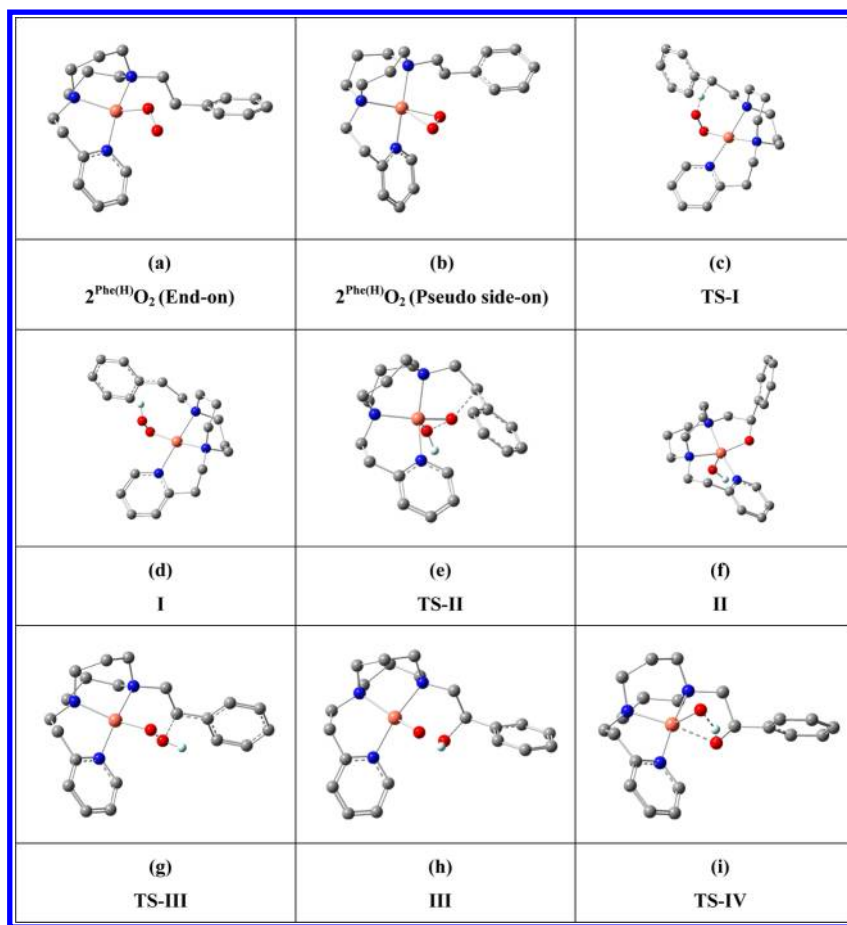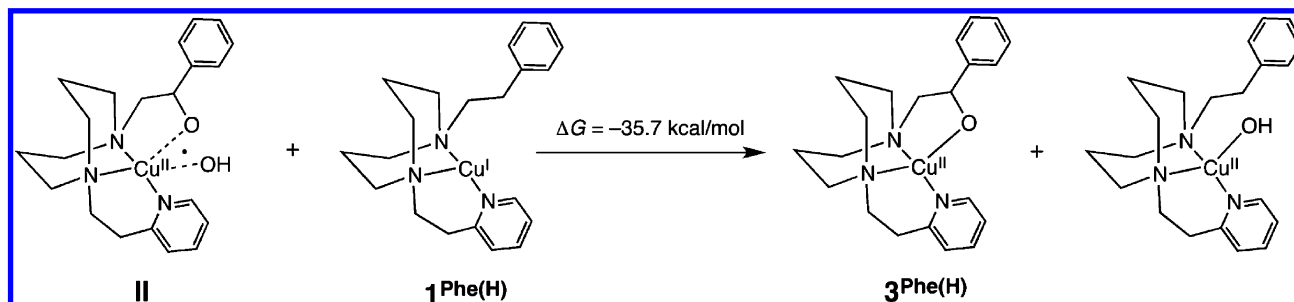
Figure 11. M11-L optimized structures of several complexes potentially relevant to the C−H bond activation reaction mechanism.

Scheme 4. Reduction of Intermediate II by Copper(I) Starting Material 1$^{Phe(H)}$ (The Final Step of the Reaction)

of −4.5 and 13.0 kcal/mol, respectively. The corresponding TS structures for hydrogen atom abstraction from the benzylic positions are associated with $\Delta G^{\ddagger}$ values of 23.1 and 16.4 kcal/mol, respectively (Figure 12). While these absolute values are lower than those predicted for the unimolecular pathway, it must be recalled that these are *standard-state* free energies, and are thus only subject to direct comparison when all species are present at 1 M concentration. As the concentration of 1$^{Phe(H)}$ is orders of magnitude smaller than 1 mol/L under experimental conditions, the formation and reactivity of dinuclear species is rendered unfavorable, although at much higher concentrations the bis-μ-oxo pathway might well begin to contribute and ultimately dominate the reactivity. In any case, theory is consistent with the observation that the ligand hydroxylation reaction displays first order kinetics and unchanging rate constant over a copper concentration range of 0.1−0.4 mM.

On the basis of these theoretical results, we conclude that ligand hydroxylation proceeds by hydrogen atom abstraction from the benzylic position initiated by the copper(II) superoxo unit of 2$^{Phe(H)}$O$_2$ followed by oxygenation of the benzylic position by the oxygen proximal to the copper center in I with concomitant O−O bond scission. Including an estimation for tunneling effects, we predict a $\Delta G^{\ddagger}$ of 20.9 kcal/mol for the key hydrogen abstraction step by 2$^{Phe(H)}$O$_2$, and we calculated the KIE for this step to be 5.6 at −65 °C, which is in fair agreement with the experimental predictions of about 16.0 kcal/mol for $\Delta G^{\ddagger}$ with a KIE of 4.1. The smaller KIE observed experimentally may indeed be due to some kinetic complexity introduced by the "rebound"-like step of benzylic oxygenation (I to **TS-II** in Figure 10) having an activation free energy similar to that for C−H abstraction. At the M-11 L level, we predict the rebound to have a somewhat higher free energy of
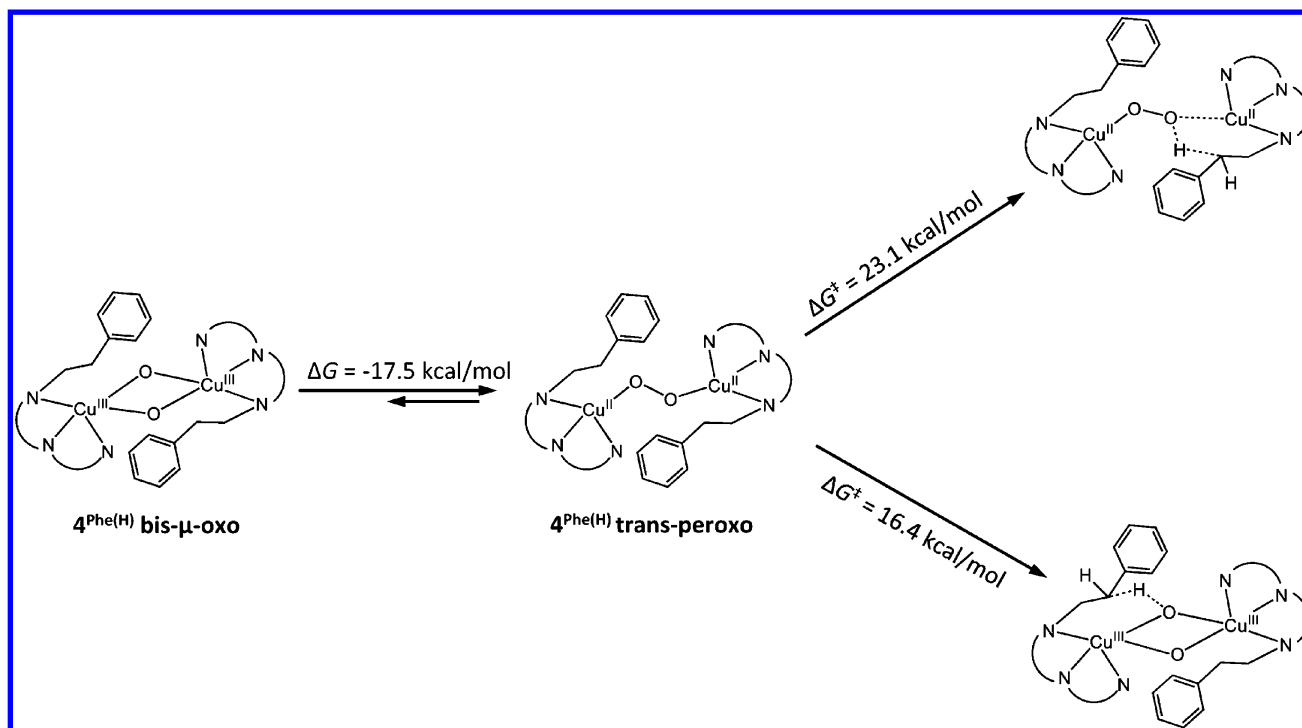
Figure 12. Reactivities of possible dinuclear species, **4$^{Phe(H)}$ trans-peroxo** and **4$^{Phe(H)}$ bis-μ-oxo**. The relative free energies at 298.15 K are reported in units of kcal/mol.

activation, but the difference of 3 kcal/mol is likely within the error of the various approximations in the theoretical model.

CONCLUSION

In this study, structures and physicochemical properties as well as reactivity of the copper(I) and copper(II) complexes supported by the new tridentate ligands L^R have been examined in detail in order to gain insight into the chemistry in the active sites of mononuclear copper monooxygenases. The ligand exhibits the unique feature that in the solid state it stabilizes the copper(I) complexes in a T-shaped geometry and the copper(II) complexes in a distorted tetrahedral geometry. The copper(II) complexes also adopt the four-coordinate structure in solution as demonstrated by the EPR spectra and by the observation that the copper(II) complexes exhibit the same spectra both in the absence and in the presence of highly coordinating co-solvents such as DMSO and DMF in CH$_2$Cl$_2$. Such a distorted tetrahedral structure of the copper(II) complexes resembles the structure of the Cu$_B$ site of the resting state of PHM.[74]

Low temperature oxygenation of the copper(I) complexes generated mononuclear copper(II) end-on superoxo complexes having an intense absorption band at ~395 nm and broad bands at 585 and 723 nm (Figure 5) and isotope sensitive O–O and Cu–O stretching vibrations of the end-on superoxo species. The superoxo complex has a triplet ground state, which has also been well confirmed by parallel mode EPR[43] and DFT calculations. Detailed kinetic analysis for the O$_2$-adduct formation reaction gave kinetic and thermodynamic parameters providing mechanistic insights into the association and dissociation processes of O$_2$ to the copper complexes.

The copper(II) end-on superoxo complex gradually decomposes to induce aliphatic ligand hydroxylation to give an alkoxocopper(II) product (Scheme 3). Kinetic studies on the decomposition reaction suggested that the superoxo complex

itself is an active species to induce the aliphatic ligand hydroxylation reaction. DFT studies at the M11-L level support that; at low copper concentrations, C–H bond abstraction occurs unimolecularly from the superoxo complex with subsequent rebound of the copper hydroperoxo species to generate an oxygenated ligand.

To date, the reactivity of several mononuclear copper(II) superoxo complexes has been examined to assess possible involvement of such species in related enzymatic reactions, but none of the superoxo copper(II) model complexes has been shown to exhibit direct C–H bond activation of organic substrates.[37,41,42] Recently, mononuclear copper(II) superoxo species has been invoked as the key intermediate in the enzymatic reactions catalyzed by PHM and DβM. The present model studies indicate that such a superoxo species could be reactive enough to induce the direct C–H bond activation of aliphatic substrates.

ASSOCIATED CONTENT

ⓢ Supporting Information

Crystallographic data in CIF format. Further details are given in Figures S1–S24 and Tables S1–S8. This material is available free of charge via the Internet at http://pubs.acs.org.

AUTHOR INFORMATION

Corresponding Author

*E-mail: shinobu@mls.eng.osaka-u.ac.jp (S.I.), cramer@umn.edu (C.J.C.).

Notes

The authors declare no competing financial interest.

■ REFERENCES

(1) Klinman, J. P. *Chem. Rev.* **1996**, *96*, 2541.

(2) Mirica, L. M.; Ottenwaelder, X.; Stack, T. D. P. *Chem. Rev.* **2004**, *104*, 1013.

(3) Lewis, E. A.; Tolman, W. B. *Chem. Rev.* **2004**, *104*, 1047.

(4) Chen, P.; Solomon, E. I. *Proc. Natl. Acad. Sci. U. S. A.* **2004**, *101*, 13105.

(5) Itoh, S. *Curr. Opin. Chem. Biol.* **2006**, *10*, 115.

(6) Cramer, C. J.; Tolman, W. B. *Acc. Chem. Res.* **2007**, *40*, 601.

(7) Roth, J. P. *Curr. Opin. Chem. Biol.* **2007**, *11*, 142.

(8) Rolff, M.; Tuczek, F. *Angew. Chem., Int. Ed.* **2008**, *47*, 2344.

(9) Punniyamurthy, T.; Rout, L. *Coord. Chem. Rev.* **2008**, *252*, 134.

(10) Himes, R. A.; Karlin, K. D. *Curr. Opin. Chem. Biol.* **2009**, *13*, 119.

(11) Pap, J. S.; Kaizer, J.; Speier, G. *Coord. Chem. Rev.* **2010**, *254*, 781.

(12) Itoh, S. In *Copper-Oxygen Chemistry*; Karlin, K. D., Itoh, S., Eds.; John Wiley & Sons: Hoboken, NJ, 2011; Vol. *4*, p 225.

(13) Prigge, S. T.; Mains, R. E.; Eipper, B. A.; Amzel, L. M. *Cell. Mol. Life Sci.* **2000**, *57*, 1236.

(14) Halcrow, M. A. In *Comprehensive Coordination Chemistry II*; Que, J., L., Tolman, W. B., Eds.; Elsevier: Amsterdam, The Netherlands, 2004; p 395.

(15) Klinman, J. P. *J. Biol. Chem.* **2006**, *281*, 3013.

(16) Hess, C. R.; Wu, Z.; Ng, A.; Gray, E. E.; McGuirl, M. A.; Klinman, J. P. *J. Am. Chem. Soc.* **2008**, *130*, 11939.

(17) Prigge, S. T.; Kolhekar, A. S.; Eipper, B. A.; Mains, R. E.; Amzel, L. M. *Science* **1997**, *278*, 1300.

(18) Prigge, S. T.; Kolhekar, A. S.; Eipper, B. A.; Mains, R. E.; Amzel, L. M. *Nat. Struct. Biol.* **1999**, *6*, 976.

(19) Evans, J. P.; Ahn, K.; Klinman, J. P. *J. Biol. Chem.* **2003**, *278*, 49691.

(20) Prigge, S. T.; Eipper, B. A.; Mains, R. E.; Amzel, L. M. *Science* **2004**, *304*, 864.

(21) Bollinger, J.; Martin, J.; Krebs, C. *Curr. Opin. Chem. Biol.* **2007**, *11*, 151.

(22) Francisco, W. A.; Wille, G.; Smith, A. J.; Merkler, D. J.; Klinman, J. P. *J. Am. Chem. Soc.* **2004**, *126*, 13168.

(23) Bauman, A. T.; Yukl, E. T.; Alkevich, K.; McCormack, A. L.; Blackburn, N. J. *J. Biol. Chem.* **2006**, *281*, 4190.

(24) Evans, J. P.; Blackburn, N. J.; Klinman, J. P. *Biochemistry* **2006**, *45*, 15419.

(25) Chen, P.; Solomon, E. I. *J. Am. Chem. Soc.* **2004**, *126*, 4991.

(26) de la Lande, A.; Parisel, O.; Gérard, H.; Moliner, V.; Reinaud, O. *Chem.—Eur. J.* **2008**, *14*, 6465.

(27) Fujii, T.; Yamaguchi, S.; Funahashi, Y.; Ozawa, T.; Tosha, T.; Kitagawa, T.; Masuda, H. *Chem. Commun.* **2006**, 4428.

(28) Fujisawa, K.; Tanaka, M.; Morooka, Y.; Kitajima, N. *J. Am. Chem. Soc.* **1994**, *116*, 12079.

(29) Chen, P.; Root, D. E.; Campochiaro, C.; Fujisawa, K.; Solomon, E. I. *J. Am. Chem. Soc.* **2003**, *125*, 466.

(30) Hong, S.; Huber, S. M.; Gagliardi, L.; Cramer, C. C.; Tolman, W. B. *J. Am. Chem. Soc.* **2007**, *129*, 14190.

(31) Fujii, T.; Yamaguchi, S.; Hirota, S.; Masuda, H. *Dalton Trans.* **2008**, 164.

(32) Izzet, G.; Zeitouny, J.; Akdas-Killig, H.; Frapart, Y.; Ménage, S.; Douziech, B.; Jabin, I.; Le Mest, Y.; Reinaud, O. *J. Am. Chem. Soc.* **2008**, *130*, 9514.

(33) Thiabaud, G.; Guillemot, G.; Schmitz-Afonso, I.; Colasson, B.; Reinaud, O. *Angew. Chem., Int. Ed.* **2009**, *48*, 7383.

(34) Schatz, M.; Raab, V.; Foxon, S. P.; Brehm, G.; Schneider, S.; Reiher, M.; Holthausen, M. C.; Sundermeyer, J.; Schindler, S. *Angew. Chem., Int. Ed.* **2004**, *43*, 4360.

(35) Würtele, C.; Gaoutchenova, E.; Harms, K.; Holthausen, M. C.; Sundermeyer, J.; Schindler, S. *Angew. Chem., Int. Ed.* **2006**, *45*, 3867.

(36) Maiti, D.; Fry, H. C.; Woertink, J. S.; Vance, M. A.; Solomon, E. I.; Karlin, K. D. *J. Am. Chem. Soc.* **2007**, *129*, 264.

(37) Maiti, D.; Lee, D.-H.; Gaoutchenova, K.; Würtele, C.; Holthausen, M. C.; Sarjeant, A. A. N.; Sundermeyer, J.; Schindler, S.; Karlin, K. D. *Angew. Chem., Int. Ed.* **2008**, *47*, 82.

(38) Jazdzewski, B. A.; Reynolds, A. M.; Holland, P. L.; Young, V. G., Jr.; Kaderli, S.; Zuberbuhler, A. D.; Tolman, W. B. *J. Biol. Inorg. Chem.* **2003**, *8*, 381.

(39) Komiyama, K.; Furutachi, H.; Nagatomo, S.; Hashimoto, A.; Hayashi, H.; Fujinami, S.; Suzuki, M.; Kitagawa, T. *Bull. Chem. Soc. Jpn.* **2004**, *77*, 59.

(40) Lanci, M. P.; Smirnov, V. V.; Cramer, C. J.; Gauchenova, E. V.; Sundermeyer, J.; Roth, J. P. *J. Am. Chem. Soc.* **2007**, *129*, 14697.

(41) Donoghue, P. J.; Gupta, A. K.; Boyce, D. W.; Cramer, C. J.; Tolman, W. B. *J. Am. Chem. Soc.* **2010**, *132*, 15869.

(42) Peterson, R. L.; Himes, R. A.; Kotani, H.; Suenobu, T.; Tian, L.; Siegler, M. A.; Solomon, E. I.; Fukuzumi, S.; Karlin, K. D. *J. Am. Chem. Soc.* **2011**, *133*, 1702.

(43) Kunishita, A.; Kubo, M.; Sugimoto, H.; Ogura, T.; Sato, K.; Takui, T.; Itoh, S. *J. Am. Chem. Soc.* **2009**, *131*, 2788.

(44) Murrayrust, P.; Murrayrust, J.; Clay, R. *Acta Crystallogr., Sect. B: Struct. Sci.* **1980**, *36*, 452.

(45) Houser, R. P.; Young, V. G.; Tolman, W. B. *J. Am. Chem. Soc.* **1996**, *118*, 2101.

(46) Bu, X. H.; Shang, Z. L.; Weng, W.; Zhang, R. H.; Zhu, H. P.; Liu, Q. T. *Acta Chem. Scand.* **1999**, *53*, 295.

(47) Bu, X. H.; Du, M.; Shang, Z. L.; Zhang, R. H.; Liao, D. Z.; Shionoya, M.; Clifford, T. *Inorg. Chem.* **2000**, *39*, 4190.

(48) Halfen, J. A.; Fox, D. C.; Mehn, M. P.; Que, L. *Inorg. Chem.* **2001**, *40*, 5060.

(49) Perrin, D. D.; Armarego, W. L. F.; Perrin, D. R. *Purification of Laboratory Chemicals*, 4th ed.; Pergamon Press: Elmsford, NY, 1996.

(50) Kryatov, S. V.; Rybak-Akimova, E. V.; Schindler, S. *Chem. Rev.* **2005**, *105*, 2175.

(51) *CRC Handbook of Chemistry and Physics*, 79th ed.; CRC Press: New York, 1998.

(52) Houser, R. P.; Young, V. G.; Tolman, W. B. *J. Am. Chem. Soc.* **1996**, *118*, 2101.

(53) Burla, M. C.; Caliandro, R.; Camalli, M.; Carrozzini, B.; Cascarano, G. L.; Caro, L. D.; Giacovazzo, C.; Polidori, G.; Siliqi, D.; Spagna, R. *J. Appl. Crystallogr.* **2007**, *40*, 609.

(54) Peverati, R.; Truhlar, D. G. *J. Phys. Chem. Lett.* **2012**, *3*, 117.

(55) Dolg, M.; Wedig, U.; Stoll, H.; Preuss, H. *J. Chem. Phys.* **1987**, *86*, 866.

(56) Hehre, W. J.; Radom, L.; Schleyer, P. V. R.; Pople, J. A. *Ab Initio Molecular Orbital Theory*; Wiley: New York, 1986.

(57) Frisch et al. *Gaussian 09*, Revision A.02; Gaussian, Inc.: Wallingford, CT, 2009.

(58) Cramer, C. J. *Essentials of Computational Chemistry: Theories and Models*, 2nd ed.; John Wiley & Sons: Chichester, U.K., 2004.

(59) Marenich, A. V.; Cramer, C. J.; Truhlar, D. G. *J. Phys. Chem. B* **2009**, *113*, 6378.

(60) Ziegler, T.; Rauk, A.; Baerends, E. J. *Theor. Chim. Acta* **1977**, *43*, 261.

(61) Noodleman, L. *J. Chem. Phys.* **1981**, *74*, 5737.

(62) Cramer, C. J.; Truhlar, D. G. *Phys. Chem. Chem. Phys.* **2009**, *11*, 10757.

(63) Yamaguchi, K.; Jensen, F.; Dorigo, A.; Houk, K. N. *Chem. Phys. Lett.* **1988**, *149*, 537.

(64) Soda, T.; Kitagawa, Y.; Onishi, T.; Takano, Y.; Shigeta, Y.; Nagao, H.; Yoshioka, Y.; Yamaguchi, K. *Chem. Phys. Lett.* **2000**, *319*, 223.

(65) Noodleman, L.; Peng, C. Y.; Case, D. A.; Mouesca, J.-M. *Coord. Chem. Rev.* **1995**, *144*, 199.

(66) Neese, F. *Coord. Chem. Rev.* **2009**, *253*, 526.

(67) Ciofini, I.; Daul, C. A. *Coord. Chem. Rev.* **2003**, *238*, 187.

(68) Harvey, J. N. *Struct. Bonding (Berlin)* **2004**, *112*, 151.

(69) Schmider, H. L.; Becke, A. D. *J. Chem. Phys.* **1998**, *108*, 9624.

(70) Improta, R.; Barone, V.; Scalmani, G.; Frisch, M. J. *J. Chem. Phys.* **2006**, *125*, 054103.

(71) The synthetic procedures of $\mathbf{L}^{\mathbf{Phe(X)}}$ (X = OMe, H, and NO_2) and their copper(I) complexes have already been reported in our previous communication.[43]

(72) Boswell, J. S.; Reedy, B. J.; Kulathila, R.; Merkler, D.; Blackburn, N. J. *Biochemistry* **1996**, *35*, 12241.

(73) Yang, L.; Powell, D. R.; Houser, R. P. *Dalton Trans.* **2007**, 955.

(74) Chufán, E. E.; Prigge, S. T.; Siebert, X.; Eipper, B. A.; Mains, R. E.; Amzel, L. M. *J. Am. Chem. Soc.* **2010**, *132*, 15565.

(75) Kitajima, N.; Fujisawa, K.; Morooka, Y. *J. Am. Chem. Soc.* **1990**, *112*, 3210.

(76) Espenson, J. H. *Chemical Kinetics and Reaction Mechanisms*; McGraw Hill, Inc.: New York, 1981.

(77) Weitzer, M.; Schindler, S.; Brehm, G.; Schneider, S.; Hormann, E.; Jung, B.; Kaderli, S.; Zuberbühler, A. D. *Inorg. Chem.* **2003**, *42*, 1800.

(78) Zhang, C. X.; Kaderli, S.; Costas, M.; Kim, E.; Neuhold, Y. M.; Karlin, K. D.; Zuberbühler, A. D. *Inorg. Chem.* **2003**, *42*, 1807.

(79) Skodje, R. T.; Truhlar, D. G. *J. Phys. Chem.* **1981**, *85*, 624.